



UiT Norges arktiske universitet

Faculty of Health Sciences

Department of Pharmacy

Drug Transport and Delivery Research Group

High throughput lipolysis-permeation *in vitro* model employing the mucus-PVPA barriers to assess drug absorption from lipid-based delivery systems

Sunniva Brurok

Thesis for the degree Master of Pharmacy 2020

MASTER THESIS FOR DEGREE OF MASTER OF PHARMACY

HIGH THROUGHPUT LIPOLYSIS-PERMEATION *IN VITRO* MODEL EMPLOYING
THE MUCUS-PVPA BARRIERS TO ASSESS DRUG ABSORPTION FROM LIPID-
BASED DELIVERY SYSTEMS

BY
SUNNIVA BRUROK
MAY 2020

SUPERVISORS
PhD student MARGHERITA FALAVIGNA
Professor GØRIL EIDE FLATEN

Drug Transport and Delivery Research group
Department of Pharmacy
Faculty of Health Sciences
UNIVERSITY OF TROMSØ - THE ARTIC UNIVERSITY OF NORWAY

ACKNOWLEDGEMENT

The work presented in this master thesis was carried out at the Drug Transport and Delivery Research Group, Department of Pharmacy, University of Tromsø - The Arctic University of Norway from September 2019 to May 2020.

First of all, I would like to thank my thesis supervisor Professor Gøril Eide Flaten for her great knowledge and for supporting me during this master project.

I also want to give my sincerest gratitude to Ph.D. student Margherita Falavigna for her continuous support in the laboratory and for always taking time to help me with whatever problems that would arise. Thank you for your patience, guidance and encouragement.

I would further like to thank the Drug Delivery Research Group for making me feel welcome and for providing a friendly and professional research environment. Especially thanks to Cristiane de Albuquerque Cavalcanti Jacobsen and Martin Skipperud Skarpeid for your kindness and for all your help in the laboratory.

Also, I would like to thank my fellow master students in the Drug Transport and Delivery Research Group, especially Julie Wik Olaussen and Ann Kristin Pettersen for their great company in the laboratory and for their encouragement. Without you this period would have never been the same. My gratitude also goes to my fellow students at the Department of Pharmacy with special thanks to Ida Marie Thomassen, Sigrid Grøttebø Hellem, Johanne Mikkelsen, Michelle Nguyen and Mac Chan for making my student years amazing.

Finally, I would like to thank my family for their endless support. Especially my Mom and Dad for always cheering me on and believing in me. I am very grateful to have parents like you.

- Sunniva Brurok, May 2020

Innholdsfortegnelse

ACKNOWLEDGEMENT	II
LIST OF FIGURES.....	VI
LIST OF TABLES	VIII
LIST OF ABBREVIATIONS	IX
ABSTRACT	X
SAMMENDRAG	XI
1 INTRODUCTION.....	1
1.1 The human gastrointestinal tract	2
1.1.1 Digestion.....	2
1.1.2 Drug absorption	6
1.2 Biopharmaceutical classification system	9
1.3 Oral lipid-based drug delivery systems.....	10
1.3.1 Lipid formulation classification system.....	11
1.3.2 Self-nanoemulsifying drug delivery systems.....	12
1.4 <i>In vitro</i> digestion models.....	13
1.4.1 Lipolysis media.....	14
1.4.2 pH-stat lipolysis model	15
1.4.3 HTP lipolysis model	16
1.4.4 <i>In vitro-in vivo</i> correlation with lipolysis models.....	16
1.5 <i>In vitro</i> permeability models	17
1.5.1 Phospholipid vesicle-based permeation assay	18
1.6 <i>In vitro</i> lipolysis-permeation models.....	21
1.7 Fenofibrate as model drug.....	22
2 AIM OF STUDY.....	24
3 MATERIALS	25
3.1 Chemicals	25
3.2 Instruments	27
3.3 Software	28
3.4 Utensils.....	28

4	METHODS.....	29
4.1	Preparation of fenofibrate-containing SNEDDS.....	29
4.1.1	SNEDDS 75%	30
4.1.2	Super-SNEDDS 150% solution	30
4.1.3	Super-SNEDDS 150% suspension	30
4.2	Preparation of permeation barriers.....	30
4.2.1	Preparation of the PVPA	30
4.2.2	Preparation of biosimilar mucus	33
4.2.3	Preparation of the mucus-PVPA barriers.....	34
4.2.4	DMSO in PBS pH 7.4.....	34
4.3	Preparation and characterization of lipolysis medium	34
4.3.1	Preparation of HTP medium.....	34
4.3.2	Preparation of HTP medium with calcein.....	35
4.3.3	Preparation of fasted state intestinal medium.....	36
4.3.4	Preparation of fasted state intestinal medium with calcein.....	36
4.3.5	Electrical conductivity measurements	36
4.3.6	Droplet size measurements	36
4.4	<i>In vitro</i> combined lipolysis-permeation	37
4.4.1	Lipolysis-permeation setup.....	37
4.4.2	PVPA barrier integrity	38
4.4.3	Assessment of <i>in vitro</i> lipolysis in the donor compartments	38
4.4.4	Sample analysis	39
4.4.5	Polarized light microscopy	41
4.4.6	Statistical evaluation.....	42
5	RESULTS AND DISCUSSION	43
5.1	<i>In vitro</i> model validation.....	43
5.1.1	Size of E80 liposomes	43
5.1.2	Mucus-PVPA barrier integrity.....	44
5.1.3	Electrical conductivity of lipolysis media	46
5.2	<i>In vitro</i> lipolysis-permeation of fenofibrate-containing SNEDDS	47
5.2.1	<i>In vitro</i> lipolysis results	47
5.2.2	<i>In vitro</i> lipolysis in the donor compartment.....	50
5.2.3	<i>In vitro</i> permeation results	52
5.2.4	<i>In vivo-in vitro</i> correlation.....	55
5.3	Comparison between the HTP medium and fasted state intestinal medium.....	58
5.3.1	Droplet size measurement.....	58
5.3.2	<i>In vitro</i> lipolysis pellet analysis	60

6	CONCLUSION	67
7	FUTURE PERSPECTIVES	68
8	REFERENCE LIST.....	69
	APPENDIX	74
	Transmission electron microscopy	74

LIST OF FIGURES

Figure 1: Illustration of the solubilization, digestion and absorption of lipids in the stomach and small intestine. (Adapted from (Berthelsen et al., 2019) with permission).....	4
Figure 2: Illustration of a cell membrane comprising the phospholipid bilayer with various proteins embedded in it. (Adapted from (Yeagle, 2016) with permission).....	7
Figure 3: The four different classes of the BCS. (Adapted from (Jarkko et al., 2008) with permission).	9
Figure 4: Illustration of the PVPA. The mixed cellulose ester filter support is shown in pink, while the liposomes are shown in blue. Small unilamellar liposomes are found into the pores, and bigger multilamellar liposomes are found on top of the filter support. (Adapted from PhD thesis of Flaten (Flaten, 2007) with permission).....	19
Figure 5: Molecular structure of fenofibrate, molecular weight 360.831 g/mol.....	22
Figure 6: Illustration of the preparation of biosimilar mucus.	33
Figure 7: Illustration of the sample preparation before HPLC analysis. The white pellet represents fenofibrate precipitation and the orange pellet represents calcein precipitation.....	41
Figure 8: Fenofibrate distribution (%) in the pellet phase (brown) and the aqueous phase (blue) during lipolysis in HTP medium at room temperature (23-25 °C) and at 37 °C of Super-SNEDDS solution 150% (A), SNEDDS 75% (B) and Super-SNEDDS suspension 150% (C). Results expressed as mean ± SD, n = 3.....	48
Figure 9: Fenofibrate distribution (%) in the pellet phase (brown) and the aqueous phase (blue) during lipolysis without stirring in HTP medium at 37 °C of Super-SNEDDS solution 150% with lipolysis (A), SNEDDS 75% with lipolysis (B), Super-SNEDDS suspension 150% with lipolysis (C), Super-SNEDDS solution 150% without lipolysis (D), SNEDDS 75% without lipolysis (E), and Super-SNEDDS suspension 150% without lipolysis (F). Results expressed as mean ± SD, n = 3.....	51
Figure 10: Cumulative amount of fenofibrate permeated across mucus-PVPA barriers A) without lipolysis and B) with lipolysis. (Results expressed as mean ± SD; n=18 (mucus-PVPA barriers)).	53
Figure 11: AUC calculated from cumulative amount of fenofibrate permeated across mucus-PVPA barriers A) without lipolysis and B) with lipolysis. (Results expressed as mean ± SD; n=18 (mucus-PVPA barriers)).	53

Figure 12: Linear relationship between the area under the plasma concentration-time curves ($AUC_{in vivo}$) and the area under the solubilization-time curves $AUC_{in vitro}$ (h·% in aqueous phase). 56

Figure 13: Linear relationship between the *in vivo* data and the *in vitro* data A) without lipolysis and B) with lipolysis. 57

LIST OF TABLES

Table 1: Lipid formulation classification system (Pouton, 2000; Pouton, 2006).....	11
Table 2: Composition of SNEDDS pre-concentrate.	29
Table 3: Composition of fenofibrate-containing SNEDDSs.	29
Table 4: Inorganic salts and amount used in 1 L PBS.....	30
Table 5: Parameters used for size measurement.	32
Table 6: Composition of lipolysis media.	35
Table 7: The apparent permeability of calcein and the electrical resistance of the mucus-PVPA barriers during lipolysis-permeation experiments. Results expressed as mean \pm SD, n=18 (mucus-PVPA barriers).	45
Table 8: EC measurements of different lipolysis media. Results expressed as mean \pm SD, n=3.	46
Table 9: <i>In vitro</i> and <i>in vivo</i> data used for <i>in vitro-in vivo</i> correlation. Results expressed as mean \pm SD, n=18 (mucus-PVPA barriers).....	55
Table 10: Size distribution by intensity of the droplets present after dispersion of SNEDDS in the two lipolysis media. Results expressed as mean \pm SD, n=6.....	59
Table 11: Pictures of pellet formed from the three fenofibrate-containing SNEDDSs during lipolysis without stirring in HTP medium or in fasted state intestinal medium with and without lipolysis.	61
Table 12: Pictures from polarized light microscopy of fenofibrate crystals (scale bar 10 μ m).	64

LIST OF ABBREVIATIONS

AUC	Area under the curve
4-BBBA	4-Bromophenylboronic acid
BCS	Biopharmaceutical classification system
BSA	Bovine serum albumin
DMSO	Dimethyl sulfoxide
DLS	Dynamic light scattering
EC	Electrical conductivity
FDA	Food and drug administration
GI	Gastrointestinal
HCL	Hydrochloric acid
HPLC	High-performance liquid chromatography
HTP	High throughput
LbDDS	Lipid-based drug delivery system
LFCS	Lipid formulation classification system
NaOH	Sodium hydroxide
PAA	Polyacrylic acid
PAMPA	Parallel artificial membrane permeation assay
P_{app}	Apparent permeability coefficient
PBS	Phosphate buffered saline
PC	Phosphatidylcholine
PDI	Polydispersity index
PVPA	Phospholipid vesicle-based permeation assay
Rpm	Rotations per minute
SD	Standard deviation
SMEDDS	Self-microemulsifying drug delivery systems
SNEDDS	Self-nanoemulsifying drug delivery system
S_{eq}	Solubility equilibrium

ABSTRACT

In vitro lipolysis models are commonly used to assess the performance of lipid-based drug delivery systems (LbDDSs) in terms of their drug absorption potential; however, this *in vitro* approach has not always shown to correlate well with *in vivo* data. Several studies suggest that adding an absorption step to the *in vitro* lipolysis model would give a better estimation of absorption for drugs incorporated in LbDDSs, and thus correlate better with *in vivo* data. In the present work an *in vitro* lipolysis-permeation model was developed to assess drug absorption from LbDDSs and to predict *in vivo* absorption data. The *in vitro* model setup consisted of high throughput (HTP) lipolysis and the mucus-PVPA barriers comprising biosimilar mucus. The functionality of the mucus-PVPA barriers during lipolysis-permeation experiments was assessed, and their ability to withstand the lipolysis conditions and maintain integrity was confirmed. The model was evaluated by testing the performance of three fenofibrate containing self-nanoemulsifying drug delivery systems (SNEDDSs) (i.e. Super-SNEDDS solution 150%, SNEDDS 75% and Super-SNEDDS suspension 150%) in terms of their drug solubilization capacity and drug permeation. For the assessment of *in vitro-in vivo* correlation, *in vivo* absorption data for the same three fenofibrate-containing SNEDDSs in rats was available from a previous study. When comparing the amount of solubilized drug from the *in vitro* lipolysis step with the *in vivo* absorption data in rats, a poor *in vitro-in vivo* correlation was obtained. However, a satisfactory correlation ($R^2 > 0.9$) was attained when comparing the *in vitro* drug permeation data after lipolysis to the *in vivo* absorption data in rats. Altogether, the constructed *in vitro* model was able to predict *in vivo* data and could thus potentially be used as a reliable HTP tool for further investigations of the performance of LbDDSs.

Keywords: Lipid-based drug delivery systems; lipolysis; permeation; high throughput; mucus-PVPA; *in vitro-in vivo* correlation.

SAMMENDRAG

In vitro lipolysemodeller blir ofte brukt for å vurdere lipidbaserte legemiddel leveringsystemer (LbDDSs) sin prestasjon i form av virkestoff absorpsjon; men denne metoden har derimot ikke alltid vist å korrelere godt med *in vivo* data. Flere studier har nevnt at ved å legge til et absorpsjonstrinn i *in vitro* lipolysemodellen vil man kunne gi et bedre estimat for absorpsjon av virkestoff fra LbDDSs, og dermed korrelere bedre med *in vivo* data. I dette arbeidet ble en *in vitro* lipolyse-absorpsjonssmodell konstruert for å vurdere absorpsjon av virkestoff fra LbDDSs. Oppsettet av *in vitro* modellen besto av en high throughput (HTP) lipolysemodell og mucus-PVPA-barrierer med biosimilar mucus. Integriteten til mucus-PVPA-barrierene ble vurdert under lipolyse og var i stand til å opprettholde integritet under lipolyseforholdene som foregikk på toppen. Modellen ble evaluert ved å teste ytelsen til tre selv-nanoemulgerende legemiddelleveringsystemer (SNEDDSs) som inneholdt fenofibrat (dvs. Super-SNEDDS-solution 150%, SNEDDS 75% og Super-SNEDDS-suspensjon 150%) i henhold til grad av lipolyse, løselighet og absorpsjon. For vurderingen av *in vitro-in vivo*-korrelasjon var *in vivo* data fra de samme fenofibrat inneholdende SNEDDSs tilgjengelig fra en tidligere publisert studie. Ved sammenligning av mengde oppløst virkestoff fra *in vitro* lipolyse med *in vivo* absorpsjonsdata fra rotter, ble det oppnådd en dårlig korrelasjon. Mens en tilfredsstillende *in vitro-in vivo* korrelasjon ($R^2 > 0,9$) ble oppnådd ved sammenligning av *in vitro* absorpsjon etter lipolyse med *in vivo* absorpsjonsdata fra rotter. Totalt sett var den konstruerte *in vitro* modellen i stand til å forutsi *in vivo* data og kan dermed potensielt brukes som et pålitelig HTP verktøy for videre undersøkelser av ytelsen til LbDDSs.

Nøkkelord: Lipid-based drug delivery systems; lipolyse; permeation; high throughput; mucus-PVPA; *in vivo-in vitro* korrelasjon.

1 INTRODUCTION

Among the various drug delivery routes, the oral route is the most frequently used, due to its unique advantages, including patient compliance and cost-effectiveness (Sastry et al., 2000). However, in comparison with other drug delivery routes, the oral route involves many challenges that the drug must overcome in order to have high bioavailability (Homayun et al., 2019). The drug must be chemically stable in acidic environment of the stomach, metabolically stable against chemical and metabolic enzymes, hydrophilic enough to dissolve/solubilize in aqueous gastrointestinal (GI) fluids and blood, and lipophilic enough to permeate through cell membranes (Patrick, 2013).

To identify whether or not a drug will be suitable for the oral route the Lipinski's rule of five, Veber's rules and/or the biopharmaceutical classification system (BCS) are generally used (Amidon et al., 1995; Lipinski et al., 2012; Veber et al., 2002). The drugs that are not considered good candidates for the oral route can improve their oral bioavailability with an appropriate drug-delivery system. Lipid-based drug delivery systems (LbDDSs) have proven to increase the bioavailability of especially drugs that have low solubility in the GI fluids (i.e. poorly water-soluble drugs, BCS class II and IV drugs) (Feeney et al., 2016). LbDDSs have a wide range of potential compositions and many different types of LbDDSs have been developed. In order to choose the LbDDSs that gives the best bioavailability of the drug, *in vitro* models can be used (Feeney et al., 2016).

In vitro models are valuable tools in early drug development to predict how drugs such as poorly water-soluble drugs, will behave when formulated in the specific drug-delivery system, and by this way choose the formulation that would lead to the best drug performance *in vivo*. Ideally, the *in vitro* model should be cost-effective, simple, compatible with high throughput (HTP) screening, and at the same time mimic the human GI environment as closely as possible to generate physiologically relevant results (Billat et al., 2017). The *in vitro* pH-stat lipolysis model is the most commonly used model for the assessment of LbDDSs performance, but it has showed poor *in vitro-in vivo* correlation in many cases (Feeney et al., 2016). For this reason, increased efforts has been applied to improve the *in vitro* models for the assessment of LbDDSs, which could provide a more accurate estimation of the LbDDSs *in vivo* performance (Feeney et al., 2016).

1.1 The human gastrointestinal tract

The human GI tract is essentially a tube starting from the oral cavity, continuing through the pharynx, esophagus, stomach and intestine to the rectum and anus. The associated organs include the liver, gallbladder and pancreas (Vertzoni et al., 2019). The primary function of the GI tract is to ingest food, digest it, and absorb nutrients, water and electrolytes while it expels the remaining waste as feces (Sherwood, 2013). Drugs, when taken orally are similarly exposed to these processes. The fate of drugs in the GI tract is mainly determined by their physicochemical properties and by the formulation that they are incorporated in.

1.1.1 Digestion

Digestion is the breakdown of structurally large molecules into small absorbable molecules. The digestion mechanism can be categorized as chemical (acid, enzymes) or mechanical (chewing, motility). For the purpose of this thesis, most emphasis will be put on lipid digestion when describing the digestion processes in the GI tract because the formulations tested were LbDDSs and the absorption of the tested drug can be affected by the lipid digestion process. The majority of lipids that humans ingest through their diet are triglycerides. After oral ingestion, these lipids are subjected to a digestion process called lipolysis, where the lipids are hydrolyzed by enzymes (lipases) that exist in various locations in the GI tract (Armand, 2007). The products resulting from the lipolysis of triglycerides are monoglycerides and free fatty acids, which can be absorbed through the intestinal epithelium (Sherwood, 2013).

1.1.1.1 Oral cavity

In the GI tract, the digestion processes are first initiated in the oral cavity by mechanically breaking down the ingested material with chewing (mastication). Further on, the ingested material is mixed with saliva, which is an aqueous mixture of minerals and proteins (McClements and Li, 2010). The protein fraction in saliva includes enzymes (e.g. lingual lipase) that lead to chemical digestion processes. The passage time in the oral cavity is relatively short, and the ingested material, also referred to as the bolus, is swallowed from the oral cavity and rapidly descends through the esophagus and into the stomach. The lipid digestion processes that are taking place in the oral cavity are often neglected in an *in vitro* digestion model, mainly because the lingual lipases from the saliva are assumed not to have a significant impact on the overall lipid digestion in the GI tract (McClements and Li, 2010).

1.1.1.2 Stomach

The stomach has a J-shaped sac-like structure and can be divided into three main regions based on structural and functional differences; the fundus (upper part) secretes gastric juices, the body (middle part) also secretes gastric juices and additionally serves as a reservoir, and the antrum (lower part) generates mechanical grinding (**Figure 1**) (Berthelsen et al., 2019). The gastric juices contain acids and enzymes (e.g. gastric lipase) involved in chemical digestion, whereas the mechanical digestion occurring in the antrum contributes to mixing of the bolus with the gastric juice. After being subjected to the different digestion processes in the stomach, the bolus is referred to as the chyme. Dietary lipids are poorly soluble in the aqueous gastric fluid, and thus tend to self-aggregate into crude lipid droplets. The acid from the gastric juice contributes to a harsh acidic environment in the stomach with pH 1-2 under fasting conditions, or pH 5-6 under fed conditions depending on the type of meal (Koziolek et al., 2018). Gastric lipase is stable at pH 2-7 but exhibits highest activity at pH 4-5.4 and contributes to 10-30% of the overall hydrolysis of the ingested triglycerides (Koziolek et al., 2018). The transfer of the chyme from the stomach to the small intestine is controlled by gastric emptying through the pyloric sphincter.

1.1.1.3 Small intestine

Most of the lipid digestion and absorption takes place in the small intestine (Sherwood, 2013). The small intestine is a tube-like structure, with a large surface area which is equivalent to a tennis court (100 m²) due to the folds, villi and microvilli structures lining its inside (Qiu et al., 2017). It can be divided into three different regions; duodenum, jejunum and ileum. The chemical digestion processes are mainly occurring in the duodenum, whereas absorption primarily takes place in the jejunum and ileum. In the duodenum, the chyme is mixed with pancreatic juice secreted from the pancreas and bile secreted from the gallbladder. The pancreatic juice contains a mixture of enzymes, including pancreatic lipase which is an enzyme that hydrolyze 40-70% of the triglycerides into free fatty acids and glycerol (Armand, 2007). Moreover, the pancreas secretes bi-carbonate ions that neutralize the acids arriving from the stomach. In this way the pH in the small intestine which is normally 6.1-7 in the fasted state, and 4.8-6.5 during fed state is preserved (Vertzoni et al., 2019).

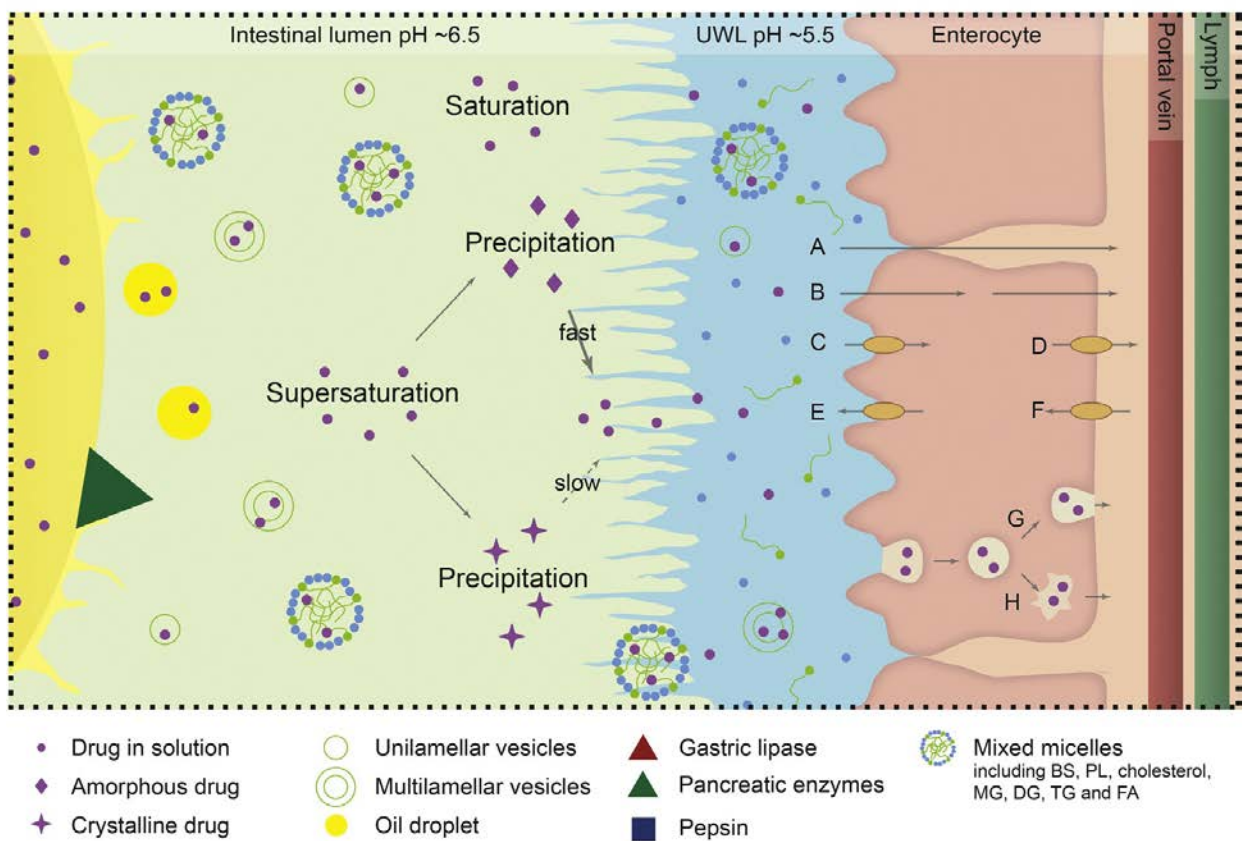
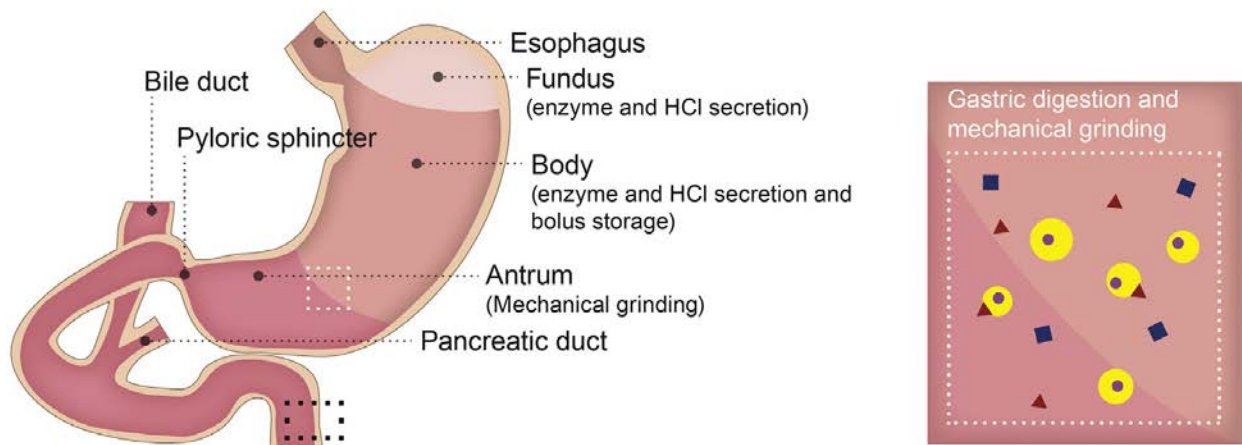


Figure 1: Illustration of the solubilization, digestion and absorption of lipids in the stomach and small intestine. (Adapted from (Berthelsen et al., 2019) with permission).

Bile primarily consists of bile salts, cholesterol, lecithin (phospholipid) and bilirubin which is produced in the liver and stored in the gallbladder (Macierzanka et al., 2019). Although the bile does not contain any digestive enzymes, it is still very important in regard to lipid digestion. Bile salts are products of bile acids conjugated with amino acids (glycine or taurine) in the liver (Macierzanka et al., 2019). Moreover, bile salts are amphipathic molecules and can adsorb on the surface of the large lipid droplets resulting from lipid self-aggregation, and thereby make the lipid droplets more stable in the aqueous intestinal fluids. The combination of bile salts and motility in the small intestine causes the crude lipid droplets to break into smaller droplets (emulsification) (Sherwood, 2013). This results in an increased surface area of the lipid droplets, which has a great impact on pancreatic lipase activity. Under physiological conditions, the pancreatic lipase enzymes are in excess compared to the substrate (triglycerides) in the small intestine, and a larger surface area (smaller droplets) will allow the binding of more pancreatic lipase to its substrate, thus increasing the rate and extent of lipolysis (Armand, 2007). However, for lipolysis to occur, the pancreatic lipase must be adsorbed on the lipid droplet surface, which is occupied by bile salts and other surface-active substances. In order to achieve this, the pancreatic lipase requires the assistance of co-lipase. Co-lipase is a co-enzyme that can adsorb on the lipid droplet surface and function as an anchor between the lipase and its substrate (Wilde and Chu, 2011).

At certain concentrations (critical micelle concentration), the lipolysis products (i.e. fatty acids and monoglycerides) and endogenous components (e.g. bile salts and phospholipids) can aggregate and form mixed micelles in the aqueous environment of the intestine (**Figure 1**) (Holm et al., 2013). The micelles formed are water-soluble because of their hydrophilic outer part, but the inner core is hydrophobic. The hydrophobic cores of the micelles have the ability to contain dissolved poorly water-soluble substances (e.g. drugs). In this way, the micelles can serve as vehicles for poorly water-soluble substances in the intestine and can be transported to their absorption sites (**Figure 1**) (Sherwood, 2013). However, the mechanisms behind the enhanced absorption observed for poorly water-soluble substances from mixed micelles are not entirely understood (Sherwood, 2013).

1.1.1.4 Large intestine

The products that have not been digested and absorbed in the upper GI-tract are transported to the large intestine where water and minerals/electrolytes are absorbed, and the remains reach the rectum and gets expelled as waste that the body cannot use.

1.1.2 Drug absorption

The small intestine is the mayor site of absorption for orally administered drugs, due to its large surface area (Qiu et al., 2017). The intestinal mucosa lines the lumen of the small intestine and is the main barrier that controls drug absorption from the lumen (Jerrold, 2009). The intestinal mucosa consists of several elements which mainly include a surface mucus layer, a cell monolayer, inner lamina propria and muscularis mucosa (Sherwood, 2013). The surface mucus layer covers the underlying epithelia and has many different functions, including protecting the epithelia from the lumen contents. The epithelial cell layer is a monolayer that mainly consists of polarized enterocytes, but other cell types (e.g. goblet cells, Paneth cells and microfold cells (M-cells)) are also present (Jerrold, 2009). The lamina propria is a thin middle layer between the epithelia and the muscularis mucosa and contains immune cells (e.g. T-cells, B-cells, macrophages, and dendritic cells) (Jerrold, 2009).

The epithelial cell layer in the small intestine has a cell membrane that consists of a phospholipid bilayer with proteins embedded into it (**Figure 2**). Phospholipids are made of a polar phosphate group head and two nonpolar fatty acid tails. The hydrophobic tails assemble in the center of the bilayer, while the hydrophilic heads make up the outer part that is in contact with the aqueous environment both inside and outside the cell (Sherwood, 2013). Embedded within the lipid bilayer are various membrane proteins (e.g. transport proteins, enzymes and receptors), that can have a variety of different roles.

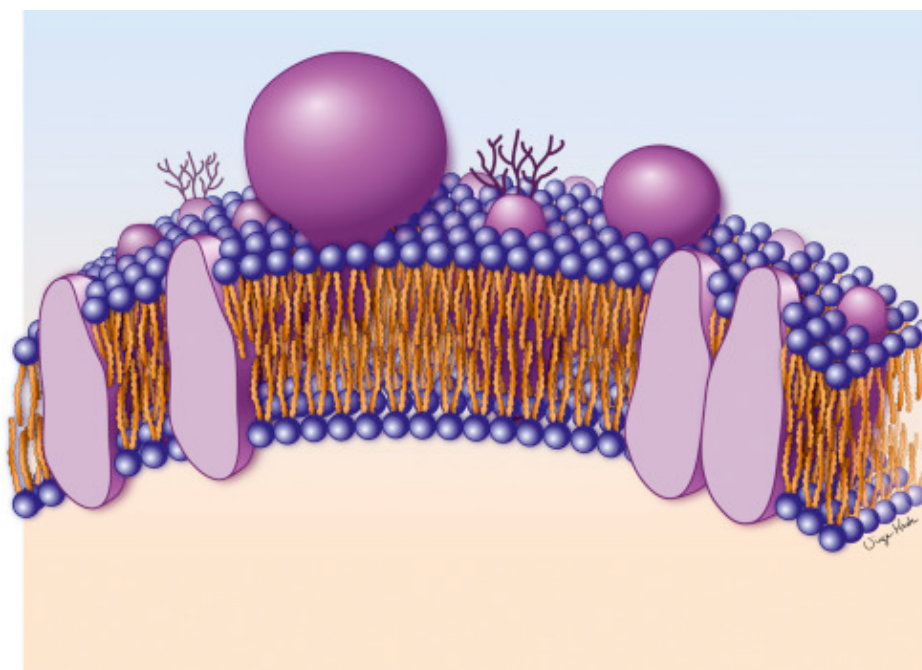


Figure 2: Illustration of a cell membrane comprising the phospholipid bilayer with various proteins embedded in it. (Adapted from (Yeagle, 2016) with permission).

1.1.2.1 Drug transport across the cell membrane

Absorption of drugs in the small intestine can occur through various mechanisms (**Figure 1 (A-H)**). The main mechanisms of drug transport across the intestinal cell layer can be divided into paracellular (**Figure 1 (A)**) and transcellular pathways. The transcellular pathways are further divided into passive diffusion (**Figure 1 (B)**), active transport (**Figure 1 (C-F)**) and endocytosis/transcytosis (**Figure 1 (G-H)**) (Berthelsen et al., 2019). The paracellular pathway allows transport of drugs through tight junctions in the intercellular space. This route is best suited for small hydrophilic drugs, due to its aqueous and narrow passage. However, the intercellular spaces in the epithelial cell layer occupy only about 0.01% of the total surface area of the intestinal epithelium, causing the paracellular route to be a relatively minor pathway for overall drug transport (Qiu et al., 2017). In passive diffusion, no energy is required and drugs can diffuse through the epithelial cell layer from a region of high concentration to a region of lower concentration (i.e. with the concentration gradient) (Qiu et al., 2017). The type of drugs that gets absorbed through passive diffusion are generally small lipophilic drugs. Another transport mechanism is active uptake, which is a transport mechanism normally facilitated by membrane proteins and requires energy (Berben et al., 2018a). The type of drugs that gets absorbed through active uptake generally have similar structure as endogenous substances (e.g.

amino acids and vitamins). Drug transport by transcytosis and endocytosis are also transport mechanisms that requires energy. In transcytosis the drug is engulfed in vesicles from the cell membrane that migrates through the cell and is ejected on the other side of the cell (Berben et al., 2018a). In endocytosis the drug is also engulfed in vesicles from the cell membrane but is transported into the cell.

1.1.2.2 Mucus layer

The surface of all epithelia throughout the GI tract is covered by a layer of mucus (Murgia et al., 2018). The mucus in the small intestine lubricates and protects the underlying epithelia from the extracellular environment in the lumen, as well as it absorbs a wide range of entities including drugs (Sherwood, 2013). The mucus is a complex hydrogel mainly composed of water (~95%) and glycoproteins (mucin) (0.5-1%), whereas other components include lipids, salts, non-mucin proteins and cell debris (Falavigna et al., 2020b). The mucins in mucus are made up by a protein backbone to which chains of glycans are attached to, creating a mesh network with a net negative charge (Boegh and Nielsen, 2015). The mesh-network functions as a steric barrier in the mucus for large compounds and particles. Moreover, the mucus has the ability to form interactions (e.g. electrostatic, hydrophobic forces and hydrogen bonds) with drugs and affects their diffusion through the mucus layer (Falavigna et al., 2020b). In general, lipophilic drugs form interactions with the non-glycosylated (naked) regions of the protein backbone in mucins, leading to a slower diffusion rate for the drug (Falavigna et al., 2020b; Sigurdsson et al., 2013).

Efforts have been made in producing artificial mucus to be used on top of *in vitro* permeability models when studying drug absorption to better mimic the intestinal mucosa. For this purpose, Boegh and colleagues developed an artificial mucus mixture, called biosimilar mucus (Boegh et al., 2014). The biosimilar mucus consists of mainly porcine mucins, lipids and proteins in buffer and is simple to prepare in the laboratory considering that no expensive or complicated equipment is required. The biosimilar mucus has shown to function as a diffusion barrier for hydrophobic drugs as well as some hydrophilic drugs and could thus be employed in *in vitro* permeability models to increase the biorelevance by more accurately mimicking the intestinal mucosa (Boegh et al., 2014).

1.2 Biopharmaceutical classification system

For drugs that are taken orally, Amidon and colleagues proposed the BCS which divides drugs into four classes based on their aqueous solubility and intestinal permeability (Amidon et al., 1995). The class in which a drug falls under can tell whether the drug is a good candidate for oral administration or not and is a valuable tool in drug development. **Figure 3** shows the four BCS classes. The solubility (X-axis, **Figure 3**) is defined in terms of the volume (ml) of water required to dissolve the highest dose strength of the drug substance at the lowest solubility within the pH range of 1–6.8 at 37 ± 1 °C. The cut of volume is set to be 250 ml, and it is supposed to reflect the so-called FDA (Food and Drug Administration) glass of water. Permeability in the BCS can be determined by various *in vivo* and *in vitro* methods (FDA, 2017). A drug substance is considered to be highly permeable if the fraction absorbed reaches $\geq 85\%$ of an administered dose, based on a mass balance determination or in comparison to an intravenous reference dose, along with evidence suggesting stability of the drug in the GI-tract (FDA, 2017).

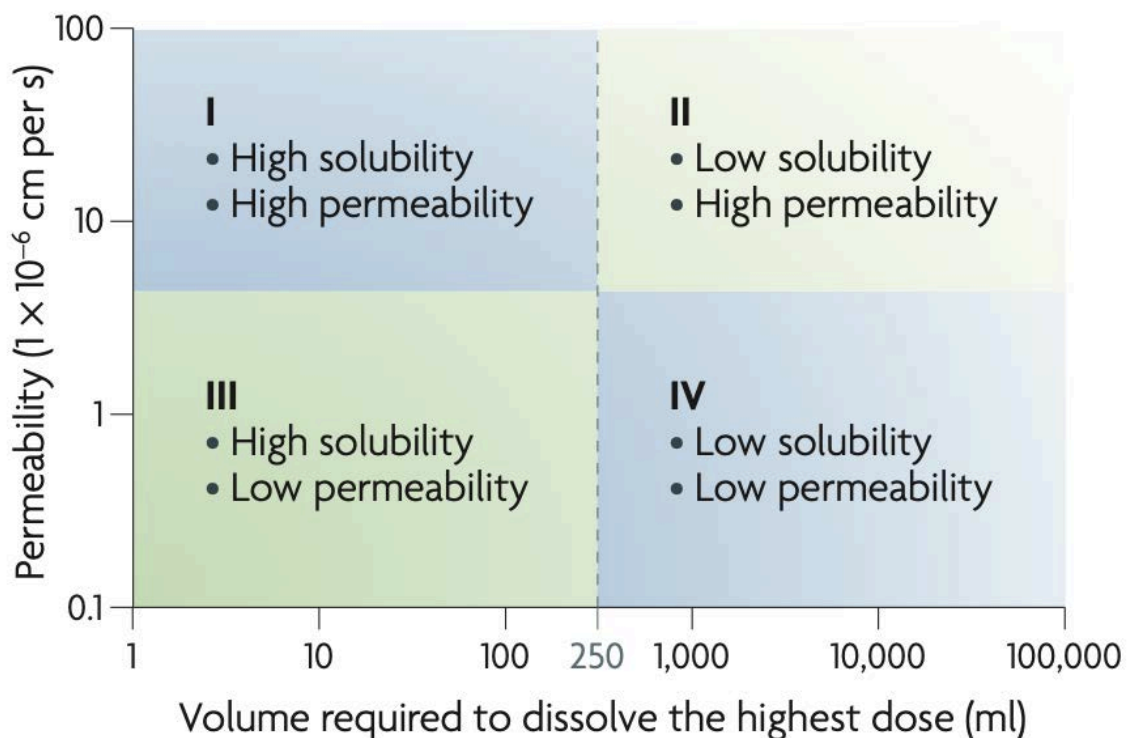


Figure 3: The four different classes of the BCS. (Adapted from (Jarkko et al., 2008) with permission).

BCS Class I drugs are usually amphiphilic compounds that exhibit both high solubility and high permeability. They are generally very well absorbed compounds and their performance can be formulation-independent. Drugs in class II are usually highly lipophilic compounds which have high permeability, but low solubility. The performance of these drugs can be modified by different types of formulation strategies, which for BCS class II drugs usually involve solubility enhancement to make them better clinical candidates for the oral route. Drugs in class III are usually hydrophilic drugs with high solubility and low permeability. For these drugs the formulation strategy aims to enhance their intestinal permeability. Class IV drugs exhibit very poor bioavailability and making these drugs into better clinical candidates for the oral route would involve a formulation strategy what would include both solubility and permeability enhancement.

1.3 Oral lipid-based drug delivery systems

The majority of new chemical entities and drugs already on the market are characterized by poor water solubility (i.e. BCS class II and IV drugs), a feature which is commonly associated with low and variable bioavailability due to a low solubilization of the drug in the GI fluids (Poovi and Damodharan, 2018). Therefore, the need of new formulation strategies has been highlighted in order to improve the bioavailability of such compounds. LbDDSs are lipid surfactant-based drug delivery systems that improve GI drug solubilization and absorption and subsequently the oral bioavailability of poorly water-soluble drugs (Feeney et al., 2016). The rationale behind the use of LbDDSs comes from the increased bioavailability seen for poor water-soluble drugs when co-administrated with food (Persson et al., 2005). Dietary lipids from food initiates physiological processes in the GI tract involving lipid digestion. Which alternately leads to the formation of various of colloid structures (e.g. mixed micelles, unilamellar and multilamellar vesicles) in the intestinal fluids that can increase the solubilization and absorption of co-administrated poorly water-soluble drugs (Porter et al., 2007).

1.3.1 Lipid formulation classification system

The lipid formulation classification system (LFCS) was proposed by Pouton and colleagues and classifies LbDDS into four main types (I-III B), based on the types and amounts of included lipids, surfactants and co-solvents (Pouton, 2000). A fifth type (IV) was introduced later due to the increasing use of formulations containing no oils nor lipids (i.e. triglycerides or mixed glycerides) (Pouton, 2006). The typical lipid composition for each type (I-IV) of LbDDS in the LFCS is presented in **Table 1**. Type I formulations are characterized by drugs dissolved in triglycerides and/or mixed glycerides. Type II formulations are water-insoluble self-emulsifying drug delivery systems (SEDDS) that comprise combinations of glycerides and lipophilic surfactants (HLB <12) (Porter et al., 2008). Type III formulations are SEDDS or self-microemulsifying drug delivery systems (SMEDDS) and can be split into type IIIA and IIIB, which differ in the proportions of lipids and water-soluble surfactants and/or co-solvents. Type IIIA contain higher portions of lipids, and lower portions of water-soluble surfactants (HLB >12) and/or co-solvents. Type IIIB contain lower portions of lipids and a greater portion of water-soluble surfactants and co-solvents. Type IV formulations include no oils and contain a combination of surfactants and co-solvents. The advantage of all these formulations lays in their ability to enhance solubilization of BCS class II and IV drugs by solubilization of the drug in their formulation and by the formation of colloid structures in the intestinal fluids that aid solubilization and absorption (Porter et al., 2008).

Table 1: Lipid formulation classification system (Pouton, 2000; Pouton, 2006).

	Type I	Type II	Type IIIA	Type IIIB	Type IV
Triglycerides or mixed glycerides (%)	100	40-80	40-80	<20	-
Water-insoluble surfactants (HLB<12) (%)	-	20-60	-	-	0-20
Water-soluble surfactants (HLB>12) (%)	-	-	20-40	20-50	30-80
Hydrophilic co-solvents (%)	-	-	0-40	20-50	0-50

1.3.2 Self-nanoemulsifying drug delivery systems

Self-nanoemulsifying drug delivery systems (SNEDDSs) are a type of LbDDS that has proved to enhance the bioavailability of poorly-water soluble drugs in several studies (Heshmati et al., 2013; Kazi et al., 2019). SNEDDSs are isotropic homogenous mixtures of oil, surfactant, co-solvent and drug, that spontaneously generate fine oil-in-water nanoemulsions in aqueous environment upon gentle agitation (Siqueira et al., 2017). The lipid formulation excipients that the drug is solubilized in, are generally referred to as the SNEDDS pre-concentrate. The properties of SNEDDS strongly depend on the choice of excipients and their ratios (Alshamsan et al., 2018). For example, the SNEDDS droplet size normally ranges from 20-200 nm, depending on several factors including the lipid used (long chain or medium chain lipids) (Thomas et al., 2012b).

One of the advantages with the SNEDDS is that the potential rate-limiting dissolution step in the GI fluids required for crystalline drugs is circumvented because the drug is already dissolved in the SNEDDS pre-concentrate. Another advantage with the SNEDDS is the small droplet size (20-200 nm), which generates a large surface area, and thereby facilitates fast and more reproducible uniform lipid digestion (Armand, 2007).

One limitation that can be associated with SNEDDSs is related to their drug loading capacity. The loading capacity is restricted by the solubility of the drug in the pre-concentrate. To compensate for low drug loading, higher amounts of formulation are normally needed to reach therapeutic doses, which in turn lead to the administration of multiple dose units, that alternately could affect patient compliance (Thomas et al., 2012a). In addition, low drug load is a problem in e.g. preclinical toxicological studies, where high drug doses are needed. Traditionally the drug load in conventional SNEDDS ranges from 50-90% of the drugs solubility equilibrium (S_{eq}) in the SNEDDS pre-concentrate (Bannow et al., 2020). Drug load at maximum drug S_{eq} (100%) in the SNEDDS has been avoided due to the concern of drug precipitation during dispersion and lipid digestion in the GI fluids (Anby et al., 2012). However, more recent studies have shown that drug precipitation from SNEDDS necessarily do not negatively affect the *in vivo* performance (Khan et al., 2016; Thomas et al., 2014). A strategy to overcome the limitation regarding drug loading in SNEDDS has been proposed by Thomas and colleagues, where the performance of supersaturated SNEDDS (i.e. Super-SNEDDS) was investigated (Thomas et al., 2012a; Thomas et al., 2012b). The Super-SNEDDS are capable of having a drug load well above the S_{eq} in the SNEDDS pre-concentrate. Super-SNEDDS containing poor water-soluble

drugs (simvastatine or halfantrine) demonstrated equivalent or improved performance *in vitro* and *in vivo* compared to conventional SNEDDS (Thomas et al., 2013; Thomas et al., 2012a).

During lipolysis, the lipids in the SNEEDS are hydrolyzed by lipase enzymes in the small intestine. The lipolysis products (i.e. fatty acids and monoglycerides) form mixed micelles and possibly other colloid structures (unilamellar and multilamellar vesicles) together with endogenous components (bile salts, phospholipids) (**Figure 1**) (Tran et al., 2017). The colloidal structures interact with the drugs and assist drug diffusion across the mucus layer, present the drug to the epithelial cell layer and facilitate its absorption (Müllertz et al., 2010).

1.4 *In vitro* digestion models

In vitro digestion models are often used to evaluate the performance of LbDDSs as the lipolysis phase is considered to be crucial for the release of the drug from the formulation and subsequently its absorption (Butler et al., 2019; Porter et al., 2007). Due to the complexity of events taking place after ingestion of LbDDSs, simple dissolution/dispersion tests are often not useful in evaluating LbDDSs as they don't account for lipid digestion (Mosgaard et al., 2015). Most *in vitro* digestion models used to evaluate LbDDSs mimic the digestion process in the stomach and intestine, but they vary in their complexity (Berthelsen et al., 2019). Simple models which only simulate the enzymatic digestion are for example the pH-stat lipolysis model and the HTP lipolysis model (Mosgaard et al., 2015; Zangenberg et al., 2001). Instead, more complex *in vitro* digestion models like the dynamic gastric test and the TNO gastro-intestinal model simulate both enzymatic and mechanical digestion (Dickinson et al., 2012; Thuenemann et al., 2015). However, the models simulating both enzymatic and mechanical digestion are very expensive and time consuming, which makes them more suitable for late phase evaluation rather than HTP screening (Berthelsen et al., 2019).

1.4.1 Lipolysis media

Simulated intestinal fluids are generally employed as the lipolysis media in *in vitro* digestion models that mimic the lipid digestion processes occurring in the intestine. Human intestinal fluids are, in fact, not practical to use as lipolysis media due to availability issues, variability in donors and in collection techniques (Khadra et al., 2015). The composition of the lipolysis medium should resemble the physiological conditions in the human intestinal fluids as close as possible. This is challenging due to the large variations in the human intestinal fluids with regard to composition, dietary state and pH (Kleberg et al., 2010). A number of various simulated intestinal fluids has been developed, and they usually contain bile salts and phospholipids in buffer at different concentrations, depending on whether they are simulating fasted or fed state conditions (Larsen et al., 2011).

In simulated intestinal fluids, bile from bovine or porcine origin has been accepted to be used as substitute for human bile. Bovine bile extract has both taurine-conjugated and glycine-conjugated bile salts, whereas porcine bile extract has mainly glycine-conjugated bile acids, but also some bile salts that are not found in humans (Larsen et al., 2011). The concentration of bile used in simulated intestinal fluids reflect the human physiological bile concentrations which is normally 2-5 mM in fasted state and 8-15 mM in fed state (Larsen et al., 2011). Phosphatidylcholine (PC) is a phospholipid that has a high abundance in human bile secretion, and it is therefore a natural choice to employ PC for the simulated intestinal medium (Bergström et al., 2014). Normally, PC obtained from egg or soybeans is used in the simulated intestinal fluids and the concentration is normally 0.1 - 0.6 mM in fasted state, and 0.1 - 4.8 mM in fed state conditions (Larsen et al., 2011). Phospholipids are secreted from the gallbladder, but they can also enter the small intestine by food ingestion. This makes the ratio between bile and phospholipids highly variable in humans, but in simulated intestinal fluids the bile-to-phospholipids ratio is generally 4 (in fasted state) (Kleberg et al., 2010). Various salts can also be added to the simulated intestinal fluid to simulate electrolytes that are also found in the human intestinal fluids and to reduce surface tension (Rezhdo et al., 2016). The pH of the lipolysis medium is also of great importance. In humans this varies depending on fasted (pH 4.8-6.5) or fed state (pH 6.1-7) (Vertzoni et al., 2019). The pH in lipolysis media is normally maintained at 6.5, which is a compromise between pH in the upper small intestine and the optimal pH for the pancreatic lipase activity (Müllertz et al., 2010).

1.4.2 pH-stat lipolysis model

The pH-stat lipolysis model is the most frequently used *in vitro* digestion model for screening of LbDDSs and has a (relatively) inexpensive and simple setup (Berthelsen et al., 2019). Different setups of the pH-stat model have been developed, and the most commonly used is the one-compartment pH-stat model simulating only intestinal lipolysis (Zangenberg et al., 2001). In this model, the lipolysis is carried out in a thermostatic vessel where the LbDDS is dispersed in simulated intestinal fluids at fixed stirring speed, ensuring homogeneity. Lipolysis is initiated by the addition of lipase enzymes, typically pancreatic lipase from porcine origin, which is found to be very similar to the human pancreatic extract (Larsen et al., 2011). The pH is continuously monitored by a pH probe coupled to a pH-stat system. Free fatty acids, liberated during the hydrolysis of triglycerides, reduce the pH of the lipolysis medium, but the pH is continuously adjusted back to the starting one via titration with NaOH, which in turn allows for the calculation of the rate and extent of lipolysis. Free fatty acids as an end product of lipolysis are able to inhibit further lipolysis; however, the addition of calcium, either continuously (the dynamic lipolysis model) (Larsen et al., 2011) or as an initial bolus (the static lipolysis model) (Larsen et al., 2011) is able to precipitate the fatty acids released during lipolysis, thereby allowing the continuation of lipolysis.

Lipolysis samples taken at specific time points during lipolysis are immediately added with a lipase inhibitor to stop further lipolysis. After centrifugation, the lipolysis samples are typically separated into three distinct phases: an oil phase, an aqueous phase and a pellet phase. The oil phase typically contains undigested drug and remaining triglycerides, and the aqueous phase contains the drug solubilized free in solution and in various colloid structures (e.g. mixed micelles, unilamellar and multilamellar vesicles). Only the free drug solubilized in the aqueous phase is considered to be available for absorption. The pellet phase contains precipitated drug (crystalline or amorphous) and insoluble calcium soaps of fatty acids. The amount of drug in each phase (i.e. drug distribution) can be quantified analytically, and the amount of drug found in the aqueous phase is assumed to be available for absorption and thus used to predict the *in vivo* performance of the LbDDS (Berthelsen et al., 2019).

1.4.3 HTP lipolysis model

A more simple lipolysis model, independent from pH titration and more suitable for HTP screening of new formulations was designed by Mosgaard and colleagues (Mosgaard et al., 2015). The configuration of the HTP model is similar to the dynamic *in vitro* lipolysis model, but the HTP model uses high concentration of the buffer Bis-Tris to obtain a high buffer capacity in the simulated intestinal medium. In this way the pH drop in the lipolysis media associated with lipolysis is avoided, and the pH of the lipolysis media stays stable throughout the experiment. For its assessment, the original HTP model was compared to the dynamic intestinal pH-stat lipolysis model. No significant difference between the models was found in terms of distribution of the drug in the different phases during lipolysis of LbDDSs containing poorly water-soluble drugs (Mosgaard et al., 2015). The original HTP model was tested in thermostated reaction vessels, but it is also applicable in 96-well setup (HTP-96) for fast assessment of LbDDSs performance (Mosgaard et al., 2017).

1.4.4 *In vitro-in vivo* correlation with lipolysis models

In vitro lipolysis models play an important role in elucidating the drug release and distribution from LbDDSs, but the models show poor *in vitro-in vivo* correlation in many cases (Feeney et al., 2016; Griffin et al., 2014; Michaelsen et al., 2019; Thomas et al., 2014). The *in vitro* lipolysis models assume that the amount of solubilized drug maintained in the aqueous phase after *in vitro* lipolysis is connected with the amount of drug that is absorbed *in vivo* (Berthelsen et al., 2019).

A possible explanation for the poor *in vitro-in vivo* correlation can be associated with the fact that in the aqueous phase after *in vitro* lipolysis the drug can be found free in solution or solubilized in colloidal structures (e.g. mixed micelles, unilamellar and multilamellar vesicles) (Berthelsen et al., 2019). Only the drug free in solution is available for absorption; however, since it is not possible to distinguish between these two types of drug solubilization in the *in vitro* lipolysis model, it is highly likely that the model overestimates how much drug is available for absorption compared to *in vivo*.

Another explanation for the poor *in vitro-in vivo* correlation could be due to the fact that the *in vitro* lipolysis setup is not mimicking the *in vivo* lumen compartment, where there is an absorption sink present (i.e. intestinal mucosa) that continuously absorbs drug from the lumen.

On the contrary, *in vitro* lipolysis models are closed systems, where the dissolved drug is not transported away from the digesting environment. This makes the *in vitro* lipolysis models unable to take into account the parallel process of drug (and lipid) absorption *in vivo* that influences the drug supersaturation in the intestinal fluids (Feeney et al., 2016). In the *in vitro* lipolysis model, the lack of the absorption step might cause supersaturation of the drug in the lipolysis medium, leading to drug precipitation *in vitro* that would not occur *in vivo*, and thereby leading to results that do not reflect what happens *in vivo* (Berthelsen et al., 2019).

1.5 *In vitro* permeability models

Drug absorption from different drug delivery systems can be assessed by various *in vitro* permeability models, that can be divided into cell-based systems and non-cell based (i.e. artificial membrane models) systems (Berben et al., 2018a). Cell-based systems, including the Caco-2 cell line derived from human colorectal adenocarcinoma (Artursson et al., 2001), have been extensively used to study intestinal drug permeation. Different types of Caco-2 models have been developed by co-culturing other cell lines together with the Caco-2 cells to achieve a cell model which more accurately represents the epithelial cell layer in the small intestine (Billat et al., 2017). Although the Caco-2 models has been considered the “gold standard” for *in vitro* permeability models, it has several drawbacks which include its complicated and time-consuming (18-21 days) preparation, making it less suitable for HTP screening. Additionally, the Caco-2 model has high inter- and intra-laboratory variability (Boyd et al., 2019).

Artificial permeation models present effective and low-cost alternatives for the assessment of drug permeation and include; the parallel artificial membrane permeation assay (PAMPA), Permeapad®, the artificial membrane insert system (AMI-system) and the phospholipid vesicle-based permeation assay (PVPA) (Berben et al., 2018a). Unlike the cell-based systems, the artificial permeation models are only capable of estimating passive diffusion of drugs. However, this is not necessarily a major drawback based on the fact that passive diffusion is the most common mechanism for the permeation of drugs (Loftsson et al., 2006). Moreover, artificial membranes have shown to be more robust against endogenous components as compared to cell-based systems (Berben et al., 2018a).

PAMPA is a HTP permeation screening assay introduced by Kansy and colleagues in 1998 (Kansy et al., 1998). The PAMPA model comprises phospholipids dissolved in organic solvent which are placed on a filter support to form a lipid barrier. In more recent years, different types of PAMPA models have been developed, with modifications in filter, lipids and transport media (Berben et al., 2018a). The PAMPA is typically applied in a 96-well plate for HTP screening.

Permeapad® is a phospholipid-based barrier with a layered structure and was first introduced by Di Cagno and colleagues in 2015 (Di Cagno et al., 2015). The Permeapad® simulates passive drug diffusion and is applicable in several permeation setups including; 96-well plates (i.e. Permeapad® plate), side-by-side diffusion chambers and conventional Franz-cells. Moreover, the Permeapad® is available in several ready-to-use formats depending on the intended permeation setup (Berben et al., 2018a).

The AMI-system is an artificial membrane which, in contrast to other cell-free permeation models, does not contain any lipids. Instead, the model consists of a regenerated cellulose membrane (molecular weight cut-off 2 kDa) mounted between two plastic rings (Berben et al., 2018b).

1.5.1 Phospholipid vesicle-based permeation assay

The PVPA is a liposome-based *in vitro* permeation model developed for medium-throughput screening of new drug candidates and formulations (Flaten et al., 2006b). The main building blocks in the PVPA are egg PC liposomes, which have a similar structure to empty cells (i.e. phospholipid bilayer surrounding an aqueous core). The liposomes are deposited into the pores and onto the surface of a porous filter support of mixed cellulose ester in order to produce a tight barrier that is able to mimic the intestinal epithelium (**Figure 4**). In contrast to other artificial membrane assays like the PAMPA model, no organic solvent is used in this model, and thus the PVPA more accurately represents the *in vivo* situation in the small intestine (Flaten et al., 2006a)

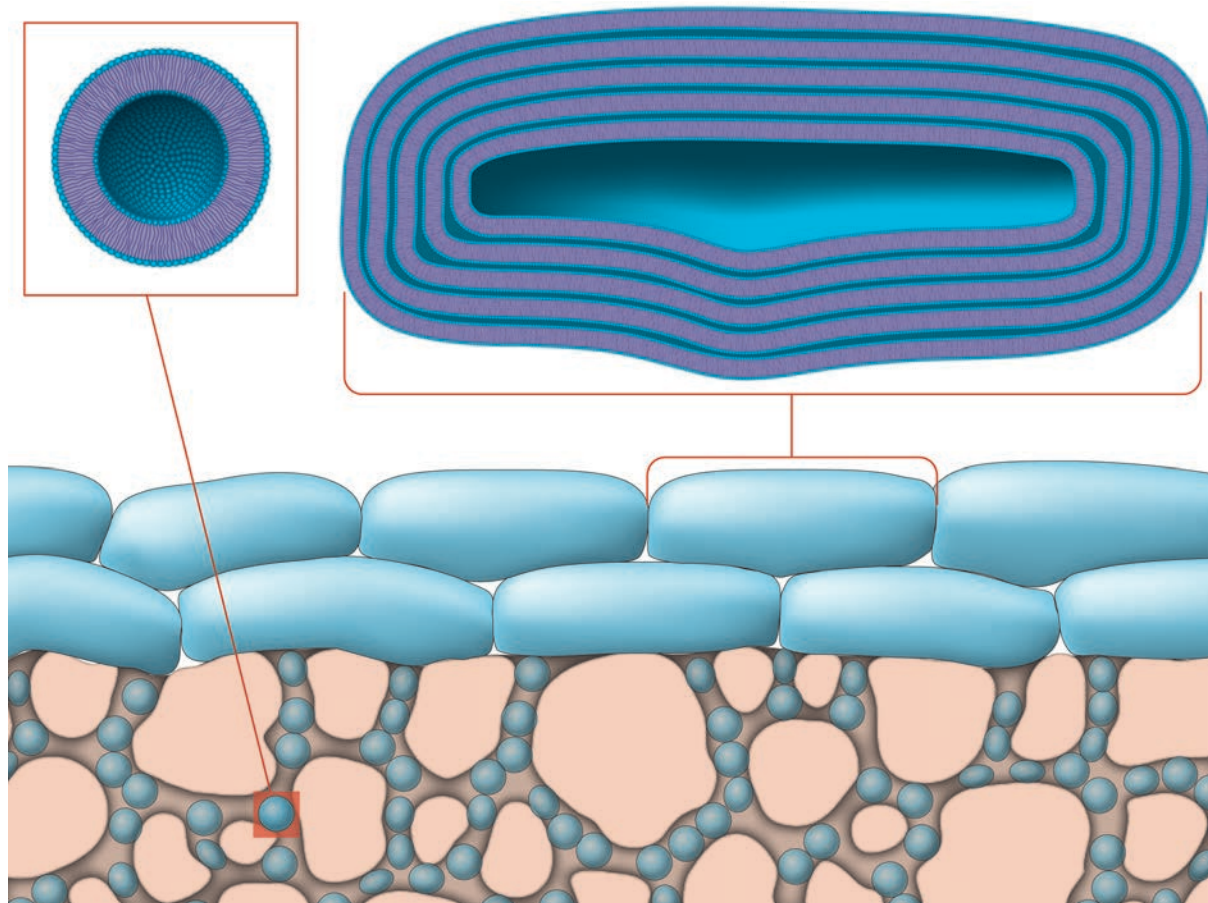


Figure 4: Illustration of the PVPA. The mixed cellulose ester filter support is shown in pink, while the liposomes are shown in blue. Small unilamellar liposomes are found into the pores, and bigger multilamellar liposomes are found on top of the filter support. (Adapted from PhD thesis of Flaten (Flaten, 2007) with permission).

The PVPA model appears to have a negligible unstirred water layer, and the permeability of compounds has proven to be unaffected by stirring or shaking (up to 100 rotations per minute (rpm)), unlike PAMPA and Caco-2 models (Flaten et al., 2007). This is due to the unique structure of the PVPA barrier, which has sponge-like properties and the water phase inside the liposomes is unaffected by the shaking or stirring of the system.

The PVPA barriers have proved to be stable within a pH range of 2.0 – 8.0, making the barriers suitable for permeation studies conducted at physiological pH in the small intestine, which is the main drug absorption site (Flaten et al., 2006a).

1.5.1.1 Mucus-PVPA

As the mucus layer is covering all mucosa tissue in humans, it is the first physiological barrier a drug has to overcome in order to be absorbed (Boegh and Nielsen, 2015). It is especially a significant barrier for poorly water soluble drugs due to its hydrophilic nature and its ability to form interactions with lipophilic drugs (Rezhdo et al., 2016). Therefore, it is essential to include the mucus barrier when studying permeation of poorly water-soluble drugs. To better mimic the composition of the intestinal mucosa in humans, a novel mucus-PVPA model was introduced (Falavigna et al., 2018). The mucus used in the mucus-PVPA consisted of unpurified mucin from porcine stomach type III and was added as a layer on top of the original PVPA barriers. The drug permeability decreased to a different extent according to the physicochemical characteristics of the drug with the mucus-PVPA compared to the original PVPA, as expected, and the mucus-PVPA model showed potential to be a reliable tool in permeability screening of drugs (Falavigna et al., 2018). Moreover, in addition to the mucus, the pH and the components in the intestinal fluids have also shown to have an impact on drug absorption in the small intestine (Mudie et al., 2010). Therefore, it would be essential to include all these factors in an *in vitro* permeation model to better mimic the *in vivo* intestinal environment and obtain physiologically relevant results. In a more recent study conducted by Falavigna and colleagues the impact of pH on drug permeation and the compatibility of the model with simulated intestinal fluids was assessed with the mucus-PVPA model (Falavigna et al., 2019). The functionality of the mucus-PVPA barriers was found to be maintained under various pH conditions and in the presence of various simulated intestinal fluids, indicating that the mucus-PVPA model can be used for drug absorption investigations in which pH and simulated intestinal fluids play a significant role (Falavigna et al., 2019).

1.6 *In vitro* lipolysis-permeation models

The commonly used pH-stat *in vitro* lipolysis model is often not able to successfully predict the *in vivo* performance of LbDDSs in terms of drug absorption (Feeney et al., 2016), and even though several promising *in vitro* permeation models has been developed, they do not take into account the lipid digestion processes occurring prior to absorption, which have proven to be of great importance for drug solubility and permeability from LbDDSs (Porter et al., 2008). Recently, a lot of attention has been put on combining *in vitro* digestion models with *in vitro* permeation models (i.e. *in vitro* lipolysis-permeation models) to get a more complete and accurate prediction of the *in vivo* performance of LbDDSs in terms of drug absorption (Feeney et al., 2016). Several attempts have been made with various combinations of *in vitro* digestion models and *in vitro* permeation models. A study by Crum and colleagues combined the pH-stat static lipolysis model with a single pass *in situ* intestinal perfusion experiment in an anaesthetised rat (Crum et al., 2016). Dahan and Hoffman conducted a study where the the pH-stat dynamic lipolysis model was combined with an *ex vivo* side-by-side diffusion chamber (Dahan and Hoffman, 2007). Bibi and colleagues used the pH-stat static lipolysis model in combination with Permeapad® in a side-by-side diffusion chamber (Bibi et al., 2017). Klitgaard and colleagues combined the pH-stat static lipolysis model with Permeapad® in Franz diffusion cells (Klitgaard et al., 2019). Moreover, the combination consisting of the pH-stat static lipolysis model and Caco-2 cells has been used to conduct several studies (Alskär et al., 2019; Keemink and Bergström, 2018; Keemink et al., 2019).

Most of the mentioned lipolysis-permeation studies did not include a mucus layer in their model. Including a mucus layer into the *in vitro* lipolysis-permeation models would mimic the intestinal mucosa more closely as the mucus layer is, in fact, the first physical barrier the drug has to overcome in the GI tract to be absorbed and has also shown to have an impact on the permeation of drugs in LbDDSs (Falavigna et al., 2018; Murgia et al., 2018). To both include the presence of mucus and to account for the impact that lipolysis has on drug absorption, a novel model was introduced by Falavigna and colleagues (Falavigna et al., 2020a). In this model, the pH-stat lipolysis model was combined with the mucus-PVPA barriers, leading to high *in vitro-in vivo* correlation for LbDDSs.

1.7 Fenofibrate as model drug

Fenofibrate is a fibric acid derivative and it is used as a lipid-lowering drug (Rang et al., 2016). Being a pro-drug, fenofibrate is hydrolyzed to its active metabolite (i.e. fenofibric acid) which acts as a PPAR α nuclear receptor agonist. Fenofibrate is a highly lipophilic BCS class II compound with a Log P 5.2 and permeates the intestinal epithelia through passive diffusion (Williams et al., 2013). Its structure is shown in **Figure 5**.

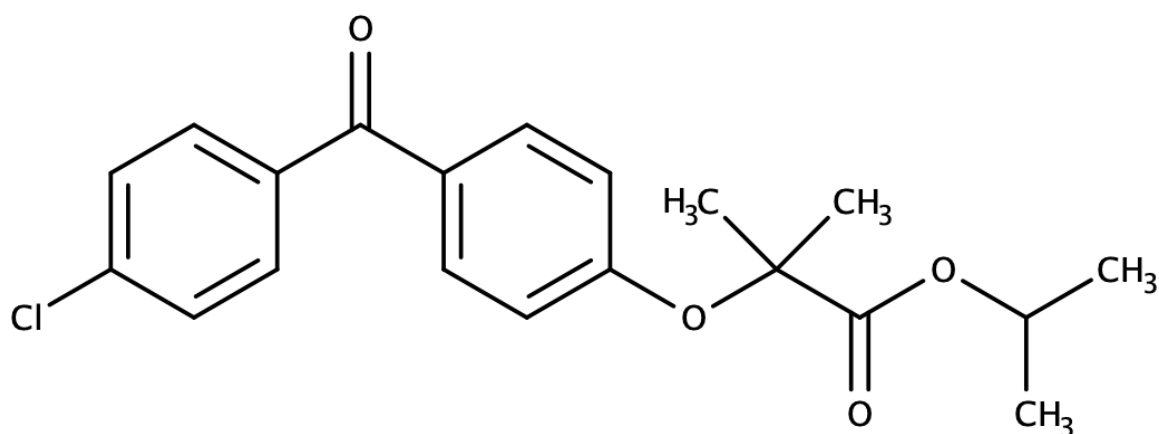


Figure 5: Molecular structure of fenofibrate, molecular weight 360.831 g/mol.

Fenofibrate was selected as a model drug for the development of a combined lipolysis-permeation model. As it is a BCS class II drug, this drug is able to be solubilized in LbDDSs such as SNEDDS, and therefore it is possible to study the effect that lipid digestion of SNEDDS has on the distribution of the drug in the aqueous and pellet phase (Williams et al., 2013). Moreover, a subsequent permeation step permits the assessment of the amount of drug available for permeation.

Michaelsen and colleagues conducted a study where they i) assessed the lipolysis of fenofibrate-containing SNEDDSs (Super-SNEDDS solution 150%, SNEDDS 75% and Super-SNEDDS suspension 150%) in an *in vitro* lipolysis setup and ii) assessed the absorption of the same fenofibrate-containing SNEDDSs in an *in vivo* study in rats (with and without the inhibition of lipolysis) (Michaelsen et al., 2019). The *in vitro* lipolysis and the *in vivo* absorption did not correlate with each other (Michaelsen et al., 2019). As previously mentioned, results obtained with the use of the *in vitro* lipolysis model does often not correlate well with *in vivo* data, and as an attempt to achieve a better correlation, an absorption step can be added to the *in vitro*

lipolysis model to assess drug absorption after *in vitro* lipolysis. This was in fact investigated in a study by Falavigna and colleagues where the same fenofibrate-containing SNEDDSs were investigated using the combined lipolysis-permeation model consisting of the pH-stat lipolysis model and the mucus-PVPA barriers (Falavigna et al 2020). This study demonstrated that a good *in vitro-in vivo* correlation could be obtained by the combination of these two setups. However, this model only produced a medium-throughput setup, where the lipolysis setup was occurring in a separate compartment compared to the permeation step, instead of having a simultaneously assessment of the two processes.

2 AIM OF STUDY

The aim of this study was to combine the HTP lipolysis model and the mucus-PVPA barriers comprising biosimilar mucus for the development of a new HTP lipolysis-permeation *in vitro* model able to predict the *in vivo* performance of SNEDDSs.

In the specific, the study focused on:

- ❖ The validation of the combined lipolysis-permeation model
- ❖ The assessment of the *in vitro* lipolysis of fenofibrate-containing SNEDDSs and the permeation of the loaded drug to predict *in vivo* drug absorption

3 MATERIALS

3.1 Chemicals

Acetonitrile ($\geq 99.9\%$) for High-performance liquid chromatography (HPLC), HiPerSolv CHROMANORM®, VWR Chemicals, USA

Bile bovine, Sigma Aldrich, St. Louis, USA

Bis-Tris ($\geq 99.0\%$), Sigma-Aldrich, St. Louis, USA

Bovine Serum Albumin ($\geq 96.0\%$), Sigma Aldrich, St. Louis, USA

4-Bromophenylboronic acid (4-BBBA), Sigma Aldrich, St. Louis, USA

Calcein, Sigma Aldrich, St. Louis, USA

Calcium chloride dihydrate ($\geq 99.0\%$), Sigma Aldrich, St. Louis, USA

Chloroform (99.0-99.4%), Sigma Aldrich, St. Louis, USA

Cholesterol ($\geq 99.0\%$), Sigma Aldrich, St. Louis, USA

Dimethyl sulfoxide (DMSO) ($\geq 99.9\%$), Sigma-Aldrich, St. Louis, USA

Ethanol (96%, v/v), AnalaR NORMAPUR®, VWR Chemicals, USA

Ethanol (99.9% v/v), Absolut alcohol prima, Arcus As, Oslo, Norway

Fenofibrate, Sigma Aldrich, St. Louis, USA

Hydrochloric acid (HCl), Sigma Aldrich, St. Louis, USA

Kolliphor RH-40, BASF, Ludwigshafen, Germany

Lipoid egg phospholipids E80 (80% PC), Lipoid GmbH, Ludwigshafen, Germany

Lipoid soybean lecithin S100 ($>94\%$ PC), Lipoid GmbH, Ludwigshafen, Germany

Magnesium sulfate ($\geq 99.5\%$), Sigma Aldrich, St. Louis, USA

Maisine CC, Gattefossé, St. Priest, France

Maleic Acid, Sigma Aldrich, St. Louis, USA

MES hydrate ($\geq 99.5\%$), Sigma Aldrich, St. Louis, USA

Methanol, for HPLC, HiPerSolv CHROMANORM®, VWR Chemicals, USA

Milli-Q filtered water

Mucin from porcine stomach, Type II, Sigma Aldrich, St. Louis, USA

Pancreatin from porcine pancreas, Sigma Aldrich, St. Louis, USA

Polyacrylic acid (Carbopol® 974PNF), Lubrizol, Brussels, Belgium

Potassium phosphate monobasic ($\geq 99.0\%$), Sigma Aldrich, St. Louis, USA

Sodium chloride, puriss. p.a. ($\geq 99.5\%$), Sigma-Aldrich, St. Louis, USA

Sodium hydroxide (NaOH), Sigma-Aldrich, St. Louis, USA

Sodium phosphate dibasic dodecahydrate ($\geq 99.0\%$), Sigma Aldrich, St. Louis, USA

Soybean oil, Sigma Aldrich, St. Louis, USA

Tween® 80, Sigma Aldrich, St. Louis, USA

Trizma® base, Sigma Aldrich, St. Louis, USA

3.2 Instruments

Accumet®, Portable pH meter kit, AP115, Fisher scientific, Massachusetts, USA

Biofuge pico centrifuge, Heraeus instrument, Kendro laboratory products GmbH, Osterode, Germany

Biofuge stratos centrifuge, Heraeus instrument, Kendro laboratory products GmbH, Osterode, Germany

Branson 5510, Branson Ultrasonic cleaner, Branson Ultrasonics Corporation, Danbury, USA

Büchi Rotavapor R-124 with Büchi Vacuum pump V-700, Büchi Vacuum controller V-85 and Büchi Water bath B-480, Büchi Labortechnik, Flawil, Switzerland

Canon DS6041, EOS 300D digital camera, Canon, Tokyo, Japan

Forma Scientific freezer 923, Forma Scientific, Inc, Marietta, USA

IBR Heat-Press, HP80-3500, IBR- Ingenierbüro, Waldkirch, Germany

Millicell-ERS, Merck Millipore, Billerica, USA

Sartorius BP211D, scale, Sartorius AG, Göttingen, Germany

SensION™⁺ PH 31, pH Meter, HACH, Düsseldorf Germany

SensION™⁺ EC 7, conductivity meter, HACH, Düsseldorf Germany

SPARK®, multimode microplate reader, Tecan Trading AG, Männedorf, Switzerland

Termarks incubator, TS 8056, Termarks AS, Bergen, Norway

Vortex Genie 2™, Bender & Hobein AG, Zurich, Switzerland

Waters Alliance 2690, HPLC separations module, Waters Corporation, Milford, USA

Waters 996, HPLC Photodiode Array Detector, Waters Corporation, Milford, USA

Zeiss Axioskop, Zeiss, Oberkochen, Germany

Zeiss objective, Plan-Neoluar 40x/0.75, Zeiss, Oberkochen, Germany

Zetasizer nanoseries, Zen 2600, Malvern Instrumentals Ltd, Malvern, UK

3.3 Software

HPLC: Millennium 32 software, version 3.20, 1999, Waters Corporation, Milford, USA

Graphpad software, version 8.4.1, Prism, San Diego, CA, USA

Microplate reader: SparkControl™, version 2.3, Tecan Trading AG, Männedorf, Switzerland

Zetasizer: Zetasizer software, version 7.13, Malvern Instrument Limited, UK

3.4 Utensils

Costar assay plate 96 well black, Corning Inc., New York, USA

Costar UV-plate 96 well transparent, Corning Inc., New York, USA

Culture inserts (d= 6.5 mm) and 24-transwell plate, Corning Inc., New York, USA

Kinetex 5 µm XB-C18 100A 100x4.6 mm HPLC-column, Phenomenex, USA

Nitrocellulose membrane filters (0.65 µm DAWP), Millipore, Billerica, USA

Nuclepore Track-Etch membrane filters (0.4 µm pore size), Whatman, Oslo, Norway

Nuclepore Track-Etch membrane filters (0.8 µm pore size), Whatman, Oslo, Norway

Ultra-High-Performance Centrifuge Tubes, 15 ml, VWR International, Leuven, Belgium

4 METHODS

4.1 Preparation of fenofibrate-containing SNEDDS

SNEDDS were used as the LbDDS for the model drug (i.e. fenofibrate) and were prepared following the method described by Michelsen and colleagues (Michaelsen et al., 2019). The SNEDDS pre-concentrate is based on long chain lipids and the composition is listed in **Table 2**. Soybean oil, Maisine CC and Kolliphor RH-40 were heated at 50 °C in a Termarks incubator. Soybean oil and Maisine CC were then mixed in a white cap glass vial on a magnetic stirrer (1:1). Subsequently, the Kolliphor RH-40 was added to the lipids and mixed until homogenous. The lipid mixture was then cooled to room temperature (23-25 °C) and absolute ethanol was added and mixed until homogenous.

Table 2: Composition of SNEDDS pre-concentrate.

Components	Amount (%w/w)
Maisine CC	27.5
Soybean oil	27.5
Kolliphor RH-40	35
Ethanol (99.9% v/v)	10

Fenofibrate-containing SNEDDSs used in the lipolysis-permeation experiments (**Table 3**) were prepared using the long chain SNEDDS pre-concentrates. The drug load is expressed as percent of the S_{eq} of fenofibrate (**Table 3**), which was previously determined by Thomas and colleagues to be 88.5 mg/g (Thomas et al., 2014).

Table 3: Composition of fenofibrate-containing SNEDDSs.

Formulations	Drug	Drug-load (%)	Concentration (mg/g)
Super-SNEDDS 150% solution	Fenofibrate	150	132.750
SNEDDS 75%	Fenofibrate	75	66.375
Super-SNEDDS 150% suspension	Fenofibrate	100 + 50	88.500 + 44.250

4.1.1 SNEDDS 75%

Fenofibrate was added to the SNEDDS pre-concentrate (66.375 mg/g) and mixed overnight at room temperature (23-25 °C) until the drug was completely dissolved in the SNEDDS pre-concentrate.

4.1.2 Super-SNEDDS 150% solution

Fenofibrate was added to the SNEDDS pre-concentrate (132.750 mg/g), mixed for 5 minutes and then ultrasonicated for 30 min in a Branson 5510, Branson Ultrasonic cleaner. Thereafter, heated for three hours at 60 °C until complete dissolution of the drug in the SNEDDS pre-concentrate and left overnight mixing at 37 °C in a Termarks incubator.

4.1.3 Super-SNEDDS 150% suspension

Fenofibrate was added to the SNEDDS pre-concentrate (88.500 mg/g) and mixed for one hour until complete dissolution. Then an additional amount fenofibrate was added (44.250 mg/g) and mixed overnight at room temperature (23-25 °C).

4.2 Preparation of permeation barriers

4.2.1 Preparation of the PVPA

4.2.1.1 Preparation of phosphate buffered saline pH 7.4

Phosphate buffered saline (PBS) pH 7.4 was prepared by weighing the inorganic salts listed in **Table 4** and dissolving them in 1 L MilliQ water. The pH of the solution was measured directly using a SensION^{TM+} pH meter, and if necessary, the pH was adjusted to 7.4 by adding adequate amounts of 1 M HCL solution and/or 1 M NaOH solution.

Table 4: Inorganic salts and amount used in 1 L PBS.

Components	Amount (g)
Potassium phosphate monobasic (KH ₂ PO ₄)	0.600
Sodium phosphate dibasic dodecahydrate (Na ₂ HPO ₄ ·12 H ₂ O)	6.400
Sodium chloride (NaCl)	7.240

4.2.1.2 Preparation of liposomes

Liposomes for the preparation of the PVPA barriers were prepared following the method described by Flaten and colleagues (Flaten et al., 2006b). Briefly, Lipoid E80 (1.8 g) was weighed in a 100 ml round bottom flask and dissolved in a 6 ml mixture of chloroform and methanol (2:1). The organic solvent was evaporated by using a Büchi Rotavapor R-124 with Büchi Vacuum pump V-700, Büchi Vacuum controller V-85 and Büchi Water bath B-480. The temperature in the water bath was set to 50 °C and the rotation at 180 rpm. When the pressure reached 700 mmHg the flask was immersed into the water bath. The organic solvent evaporated for 30 min at 200 mmHg, and then for another 30 min at 55 mmHg. Subsequently, the flask was raised out of the water bath, and evaporated for 1.5 hours in room temperature (23-25 °C). The lipid film was re-dispersed in PBS pH 7.4 containing 10% (v/v) ethanol 96% (v/v), to obtain a 6% (w/v) liposomal dispersion. Manual mixing was required in order to dislodge the lipid film present in the inside walls of the round bottom flask.

4.2.1.3 Size reduction

The liposomes were extruded by hand using syringe filter holders and Nuclepore Track-Etch membrane filters with pore sizes at 0.8 µm and 0.4 µm. In order to obtain liposomes with two different size distributions, the liposome dispersion (30 ml) was extruded five times through the 0.8 µm filter, and one portion (20 ml) was additionally extruded five times through the 0.4 µm filter.

4.2.1.4 Size analysis

The size of the liposomes after extrusion was measured by dynamic light scattering (DLS) using a Malvern Zetasizer. Prior to analysis the liposome dispersions were diluted 1:20 (v/v) with PBS pH 7.4. The measurement parameters used are presented in **Table 5**. The size of the liposomes was calculated from the mean diameter of the three measurements of each sample.

Table 5: Parameters used for size measurement.

Parameters	
Sample dispersant	Water
Viscosity	0.8872 cP
Temperature	25.0 °C
Measurement angle	173 ° backscatter
Cell type	Disposable cuvettes (DTS0012)
Number of measurements	3
Measurement duration	Automatic

4.2.1.5 Preparation of PVPA barriers

The PVPA barriers were used as the permeation tool for the permeability experiments and were prepared following the method described by Flaten and colleagues (Flaten et al., 2006b). Briefly, cellulose ester filters were fused to the base of filter inserts for 30 seconds at 150 °C by using an IBR Heat-Press. The inserts were placed into wells in 24-well plates, and 100 µl of (0.4 µm) liposomal suspension was added to each insert. Following this, the well plates were covered with lids and centrifuged at 2000 rpm for 4 minutes at 25 °C in a Biofuge stratos centrifuge. Thereafter, the inserts were transferred into new well plates, and the sequence was repeated by adding an additional 100 µl of (0.4 µm) liposomal suspension to each insert, covering the plates with lids and centrifuging under the same conditions (i.e. 2000 rpm for 4 minutes at 25 °C) for 10 minutes. After centrifugation, the inserts were placed on a sheet of paper in order to remove excess liquid, followed by the transfer to new well plates. The plates were covered with lids and then incubated for 45 minutes at 50 °C in a Termarks incubator. The inserts attained room temperature (23-25 °C) prior to the addition of 100 µl of (0.8 µm) liposomal suspension to each insert. Following this, the well plates were covered with lids and centrifuged at 2000 rpm for 30 minutes at 25 °C. With a sheet of paper placed under the lids, the plates were further centrifuged upside down at 300 rpm for 5 minutes at 25 °C. Damaged barriers were removed and the batch was stored in a Forma Scientific freezer at -75 °C, for minimum one hour and for no longer than two weeks (Flaten et al., 2006a).

Preparation of the barriers before permeation experiments was conducted by thawing the frozen barriers at 65 °C in a Termarks incubator for 30 minutes, but without lids on the plates during the last 5 minutes. If the barriers were partly wet after 30 minutes, the process was prolonged until complete dryness was observed.

4.2.2 Preparation of biosimilar mucus

Biosimilar mucus was prepared following the method described by Boegh and colleagues (Boegh et al., 2014). The preparation of biosimilar mucus is illustrated in **Figure 6**. Polyacrylic acid (PAA) (90 mg) was dissolved in 9 ml non-isotonic buffer (10 mM MES, 1.3 mM CaCl₂, 1.0 mM MgSO₄). Mucin (500 mg) was then added and stirred until dissolved, resulting in a beige mucus mixture. Then, 130 µl of 1 M NaOH were added to the solution to increase pH and viscosity. A lipid solution was prepared by mixing S100 lipids (0.18% w/v), cholesterol (0.36% w/v), and Tween 80 (0.163% w/v) in 1.1 ml of isotonic buffer (10 mM MES, 1.3 mM CaCl₂, 1.0 mM MgSO₄, 137 mM NaCl) until homogenous and 1 ml of the lipid solution was then added to the mucus mixture. Thereafter, bovine serum albumin (BSA) (310 mg) was added and stirred until homogeneously dispersed. Lastly the pH was adjusted to 6.5 with 1 M NaOH. The biosimilar mucus was stored at 4 °C when not in use. Each batch of biosimilar mucus was made a day in advance of the experiments and could be used for a maximum of 72 hours after preparation.

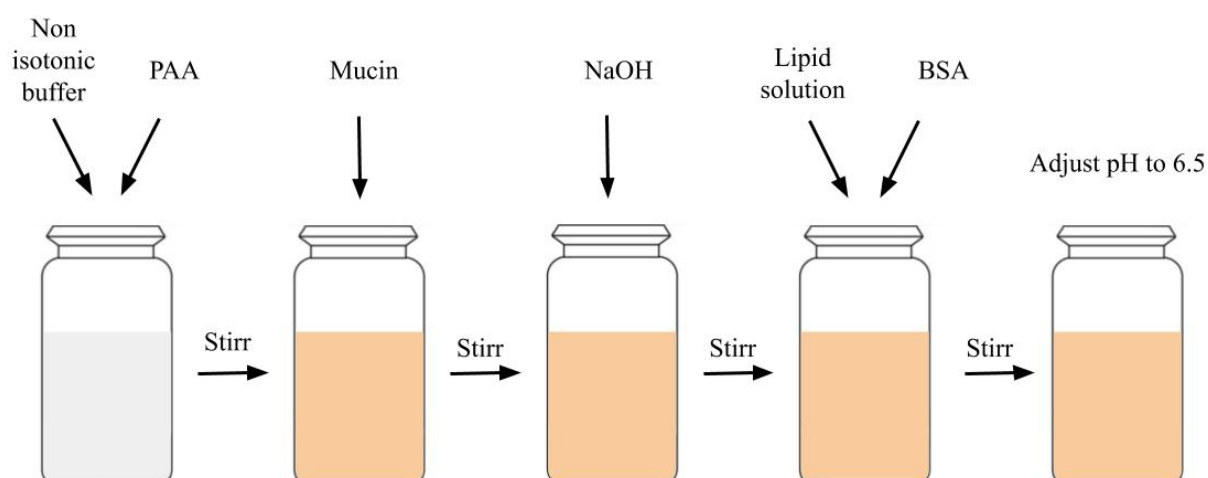


Figure 6: Illustration of the preparation of biosimilar mucus.

4.2.3 Preparation of the mucus-PVPA barriers

The preparation of the mucus-PVPA barriers was carried out prior to each lipolysis-permeation experiment. Previously prepared PVPA-barriers needed for the experiment were thawed (Section 4.2.1.5). Thereafter, biosimilar mucus (50 μ l) was applied to each barrier carefully using a 1 ml syringe. The mucus-PVPA barriers were left to incubate for 5 minutes prior to further use (Falavigna et al., 2019).

4.2.4 DMSO in PBS pH 7.4

DMSO in PBS (40 mg/ml) was chosen to be used as the acceptor medium for the permeation experiments, as it has previously shown to significantly increase the solubility of fenofibrate and thereby allowing a simpler quantification of fenofibrate permeated across the barriers (Falavigna et al., 2020a). DMSO in PBS (40 mg/ml) was prepared by solubilizing 40.00 g DMSO in 1 L of PBS pH 7.4 described in Section 4.2.1.1. The pH was measured by using a SensION^{TM+} pH meter and was adjusted to 7.4 by adding adequate amount of 1 M HCL solution and/or 1 M NaOH solution.

4.3 Preparation and characterization of lipolysis medium

4.3.1 Preparation of HTP medium

HTP medium was prepared following the method described by Mosgaard and colleagues (Mosgaard et al., 2015). HTP medium was prepared by weighing the components listed in **Table 6** and dissolving them in MilliQ water. The pH was measured directly by using a SensION^{TM+} pH meter and was adjusted to 6.5 by using 5 M HCL solution. The medium was prepared one day in advance of the lipolysis-permeation experiment and was stored in a Termarks incubator at 37 °C. The medium could be used for maximum 72 hours after preparation.

Table 6: Composition of lipolysis media.

Components	HTP medium concentrations	HTP medium with calcein concentrations	Fasted state intestinal medium concentrations	Fasted state intestinal medium with calcein concentrations
Bile bovine	2.96 mM	2.96 mM	2.95 mM	2.95 mM
Phospholipids (PC S100)	0.26 mM	0.26 mM	0.26 mM	0.26 mM
Calcium chloride dihydrate (CaCl ₂ ·2 H ₂ O)	4.50 mM	4.50 mM	1.40 mM	1.40 mM
Bis-Tris	200 mM	200 mM	-	-
NaCl	-	-	146.80 mM	146.80 mM
Maleic Acid	-	-	2.00 mM	2.00 mM
Tris	-	-	2.00 mM	2.00 mM
Calcein	-	5.00 mM	-	5.00 mM

4.3.2 Preparation of HTP medium with calcein

HTP medium with calcein was prepared by dissolving calcein (5 mM) in HTP medium (**Table 6**). The HTP medium with calcein was prepared one day in advance of the lipolysis experiments and was left to stir at 37 °C in a Termarks incubator overnight to ensure that the calcein was completely dissolved. The following day the pH was measured directly by using a SensION^{TM+} pH meter and adjusted to 6.5 by using 5 M NaOH solution and/or 5 M HCL solution. The medium was stored in a Termarks incubator at 37 °C and could be used for maximum 72 hours after preparation.

4.3.3 Preparation of fasted state intestinal medium

The preparation of fasted state intestinal medium is based on the method by Falavigna and colleagues (Falavigna et al., 2020a). Fasted state intestinal medium was prepared by weighing the components listed in **Table 6** and dissolving them in MilliQ water. The medium was stirred for minimum 3 hours in a Termarks incubator at 37 °C. Thereafter, the pH was measured directly by using a SensION™⁺ pH meter and adjusted to 6.5 by using 1 M HCL solution. The medium was stored at 37 °C while stirring and could be used for maximum 72 hours after preparation.

4.3.4 Preparation of fasted state intestinal medium with calcein

Fasted state intestinal medium with calcein was prepared by dissolving calcein (5 mM) in fasted state intestinal medium (**Table 6**). The medium was prepared one day in advance of the lipolysis experiments and was let to stir in a Termarks incubator at 37 °C overnight. The following day the pH was measured directly by using a SensION™⁺ pH meter and adjusted to 6.5 by using 5 M NaOH and/or 5 M HCL and the volume was finally adjusted. The medium was stored in a Termarks incubator at 37 °C and could be used for maximum 72 hours after preparation.

4.3.5 Electrical conductivity measurements

The electrical conductivity (EC) of all the lipolysis media listed in **Table 6** was measured with a SensION™⁺ conductivity meter at room temperature (23-25 °C). The electrode was dipped into the lipolysis medium while it reached equilibrium, and the value of the EC (mS/cm) was recorded when the reading was stable.

4.3.6 Droplet size measurements

The droplet size of the SNEDDS after dispersion in HTP medium with calcein and fasted state intestinal medium with calcein was measured by DLS using a Malvern Zetasizer. The dispersions were made with a concentration of 1.45 mg/ml of SNEDDS in each lipolysis medium (either HTP medium with calcein or fasted state intestinal medium with calcein). The samples were stirred for 10 min to ensure homogeneity prior to each DLS measurement following the method described by Mosgaard and colleagues (Mosgaard et al., 2015). The measurement parameters used were the same as in Section 4.2.1.4 and are presented in **Table 5**.

4.4 *In vitro* combined lipolysis-permeation

4.4.1 Lipolysis-permeation setup

The lipolysis of the fenofibrate-containing SNEDDSs (i.e. Super-SNEDDS solution 150%, SNEDDS 75% and Super-SNEDDS suspension 150%) was conducted in a Termarks incubator at 37 °C to simulate physiologically relevant temperature (i.e. 37 °C) and at room temperature (23-25 °C). This was done to assess if the different temperatures would have an impact on the distribution of fenofibrate during lipolysis to further consider if the experiment could be carried out at room temperature (23-25 °C). The fenofibrate-containing SNEDDSs (i.e. either Super-SNEDDS solution 150%, SNEDDS 75% or Super-SNEDDS suspension 150%) was weighed in a 50 ml beaker (“lipolysis vessel”) and dispersed in 26 ml of HTP medium with calcein (heated to 37 °C) to produce a fenofibrate concentration of 480 µg/ml. After 20 minutes of mixing the fenofibrate-containing SNEDDS in the lipolysis vessel, lipolysis was initiated by the addition of 4 ml freshly prepared pancreatic extract to yield a volume of 30 ml. The pancreatic extract was prepared by weighing porcine pancreatin (0.410 g) in a 15 ml Ultra-High-Performance centrifuge tube and adding 5 ml HTP medium pH 6.5 (previously heated to 37 °C). The mixture was vortexed until homogenous followed by centrifugation at 5000 rpm for 7 minutes at 24 °C. The pancreatic extract was used within 15 minutes to avoid denaturation of the lipase. Samples for lipolysis analysis (1 ml) were taken before the start of lipolysis (0 min), and after initiation of lipolysis at the time points 30 min and 6 hours. Lipase activity in the withdrawn samples was immediately inhibited by the addition of 5 µl lipase inhibitor (1 M 4-BBBA in methanol) followed by vortexing of the samples.

Samples for permeation (1 ml) were taken before the start of lipolysis (0 min) and 2 minutes after initiation of lipolysis. This was done to get two sets of results from fenofibrate permeation; one with lipolysis and one without lipolysis. The setup for the permeation experiment consisted of 24-well plates, used as acceptor compartments and inserts containing mucus-PVPA barriers used as donor compartments. The permeation samples (without lipolysis or with lipolysis) (100 µl) were carefully added on top of the biosimilar mucus layer in the donor compartment of the PVPA barrier in order to prevent mixing of the two layers. The permeation experiment was initiated by transferring the inserts into separate acceptor compartments (24-well plates) containing 600 µl DMSO 40 mg/ml in PBS pH 7.4. The permeation experiment was carried out at 37 °C in a Termarks incubator for 6 hours. Every second hour the inserts were transferred into fresh wells containing an equal quantity DMSO 40 mg/ml in PBS pH 7.4 to maintain sink

conditions. At the end of the permeation experiment, samples (200 μ l) were taken from each acceptor compartment for the quantification of fenofibrate.

4.4.2 PVPA barrier integrity

Immediately after *in vitro* lipolysis-permeation, the electrical resistance across the barriers was measured to evaluate their integrity, as it gives an indication on how compact the barriers are. The electrical resistance was measured by using Millicell-ERS. From the measured electrical resistance, a value of 119 Ω resulting from the cellulose filters was subtracted, and that value was then multiplied by the surface area (0.33 cm^2) of the inserts to normalize for the barrier surface area (Flaten et al., 2006a). Barriers that had an electrical resistance below 290 $\Omega \cdot \text{cm}^2$ were excluded as this value has previously shown to indicate loss of barrier integrity (Flaten et al., 2008).

The fluorescent marker calcein was added to the lipolysis media prior to the lipolysis-permeation (Section 4.3.2). The apparent permeability coefficient (P_{app}) of calcein was measured as it can give an indication of the barrier integrity. In barriers that are considered intact, calcein is expected to have low permeability due to its hydrophilic nature. Barriers that had an calcein P_{app} greater than $0.06 \cdot 10^{-6}$ cm/s were excluded as this could be associated with leakage of the barrier and loss of barrier integrity (Flaten et al., 2008).

4.4.3 Assessment of *in vitro* lipolysis in the donor compartments

As the evaluation of the lipolysis occurring directly on top of the PVPA barriers was not possible due to low donor volume, the lipolysis assessment of the lipolysis-permeation experiment took place in a lipolysis vessel consisting of a 50 ml beaker with controlled magnetic stirring (Section 4.4.1). However, in the donor compartment on top of the mucus-PVPA barriers, there was no stirring involved. Moreover, the permeation was assessed both without lipolysis and with lipolysis for each formulation (Section 4.4.1). Therefore, to study what happened on top of the mucus-PVPA barriers during permeation either without lipolysis or with lipolysis, the amount of drug solubilized was assessed in lipolysis setups where i) no stirring was applied, and ii) no stirring was applied and no pancreatin was added.

4.4.3.1 *In vitro* lipolysis without stirring

In vitro lipolysis was performed following the same method as previously described in Section 4.4.1 with some modifications. The lipolysis was conducted at 37 °C without stirring for 6 hours, and the permeation part was excluded. The lipolysis vessels were only put on the magnetic stirrer for 20 minutes prior to the addition of pancreatin extract, for 10 seconds after the addition of pancreatin extract, and 10 seconds before samples were taken to ensure homogeneity. Lipolysis without stirring was performed both with HTP medium with calcein and with fasted state intestinal medium with calcein.

4.4.3.2 *In vitro* lipolysis without stirring and without pancreatin

In vitro lipolysis without stirring and without pancreatin was performed following the same method as previously described in Section 4.4.3.1 with some modifications. The pancreatic extract was replaced with 4 ml lipolysis media (HTP medium or fasted state intestinal medium).

4.4.4 Sample analysis

4.4.4.1 Permeation samples

The permeability of calcein was determined by measuring the fluorescence of calcein from the acceptor compartments in the 24-well permeation plates by using a SPARK® multimode microplate reader at 24 °C with excitation wavelength 485 and emission wavelength 520 nm. A blank was subtracted from the fluorescence values, consisting of pure DMSO 40 mg/ml in PBS pH 7.4. The calcein calibration curve used for quantification was received. To prepare a calcein calibration curve a stock solution of calcein (20 nmol/ml) in PBS pH 7.4 was made. From this, six standard solutions (0.10, 0.80, 1.50, 3.00 and 5.00 nmol/ml) were prepared and measured using a SPARK® multimode microplate reader.

The fenofibrate permeation samples were transferred into Costar 96-well transparent UV-plates and analyzed with a SPARK® multimode microplate reader. Fenofibrate was quantified by measuring the absorbance at 288 nm wavelength at 24 °C. A blank consisting of pure DMSO 40 mg/ml in PBS pH 7.4 was subtracted from the fenofibrate absorbance values. To prepare a fenofibrate calibration curve, six standard solutions of fenofibrate (0.06, 0.24, 0.60, 2.40 and 6.00 nmol/ml) in a mixture of PBS pH 7.4 and ethanol 96% (1:1) were made and measured using a SPARK® multimode microplate reader.

4.4.4.2 Permeability calculation

The cumulative amount of permeated drug was plotted as a function of time. Steady state flux was calculated from the slope of the linear part of the curve. The obtained flux values were used to calculate the P_{app} using Equation 1:

$$P_{app}(cm/s) = \frac{J}{AC_d} \quad (\text{Equation 1})$$

Where J is the steady state flux (nmol/s), A is the surface area of the insert (cm²) and C_d is the concentration of drug in the donor (nmol/ml) (Flaten et al., 2006b).

4.4.4.3 Lipolysis samples

Two samples (T-sample and A-sample) were prepared from each lipolysis sample (0 min, 30 min and 6 hours). The T-sample contained the total amount of fenofibrate from the lipolysis sample (i.e. precipitated plus solubilized in the aqueous phase), and the A-sample contained the amount of fenofibrate solubilized in the aqueous phase. The sample preparation is illustrated in **Figure 7**. Briefly, the T-samples were prepared by transferring 100 µl from the lipolysis sample to a 2 ml Eppendorf tube containing 900 µl methanol (1:10 dilution). The T-sample (1:10 dilution) and the lipolysis sample was then centrifuged at 13 000 rpm for 10 minutes at 25 °C. Following this, the supernatant (100 µl) of the two samples was transferred to new 2 ml Eppendorf tubes containing 900 µl methanol and was once more centrifuged at 13 000 rpm for 10 minutes at 25 °C. With a final dilution of 1:100 the preparation of the T-sample was complete, whereas the A-sample was diluted once more 1:10 with methanol in order to obtain a final dilution of 1:100.

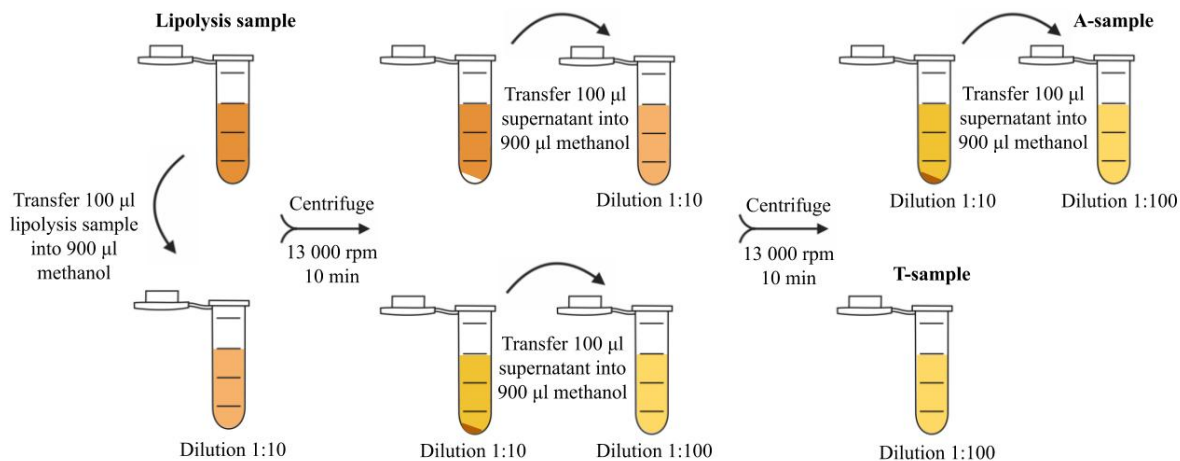


Figure 7: Illustration of the sample preparation before HPLC analysis. The white pellet represents fenofibrate precipitation and the orange pellet represents calcein precipitation.

4.4.4.4 HPLC analysis

Quantitative analysis of fenofibrate in the *in vitro* lipolysis samples (T-samples and A-samples) was performed by HPLC. This method was based on the method developed by Michelsen and colleagues (Michaelsen et al., 2019). The HPLC analysis was carried out using Waters Alliance 2690 separations module, Waters 996 PDA Detector and Phenomenex Kinetex 5u C18 100A column (100 × 4.6 mm). Fenofibrate was analyzed at a wavelength of 288 nm with a mobile phase consisting of 80% methanol and 20% water, eluted at a flow rate at 1.0 ml/min and an injection volume of 10 µl. To prepare a fenofibrate calibration curve for HPLC a stock solution of fenofibrate (400 µg/ml) in methanol was diluted 0.3:10, resulting in a stock solution with a fenofibrate concentration of 12.00 µg/ml. From this, six standard solutions (0.06, 0.24, 0.60, 2.40 and 6.00 µg/ml) were prepared.

4.4.5 Polarized light microscopy

Microscopic analysis of selected pellets containing precipitated fenofibrate crystals after lipolysis without stirring (Section 4.4.3.1), and without stirring and pancreatin (Section 4.4.3.2) was conducted using a Zeiss Axioskop. The microscopic analysis was carried out to investigate the morphology of the fenofibrate crystals. Samples for the microscopy analysis were prepared by carefully removing the pellet from the lipolysis sample and placing them on a microscope slide. The samples were observed at a magnification of 40× with a Zeiss Plan-Neofluar

objective and all images were taken with the same magnitude by using a Canon DS6041 digital camera.

4.4.6 Statistical evaluation

GraphPad Prism 8.4.1 was used for the statistical analysis of the data. One-way ANOVA was employed when comparing three or more sets of data and student t-test was employed when comparing two sets of data ($p < 0.05$).

5 RESULTS AND DISCUSSION

5.1 *In vitro* model validation

The validation of the new combined *in vitro* lipolysis-permeation model was conducted to confirm that the model could meet its predetermined specifications, and thereby ensure the functionality of the components employed in the new model setup. A set of control experiments was carried out for the *in vitro* model validation.

5.1.1 Size of E80 liposomes

In order to obtain liposomes with two different size distributions for the preparation of the PVPA barriers, the liposome dispersions were extruded by membrane filters with pore sizes of 400 nm and 800 nm (Section 4.2.1.3). The liposomes extruded through filters with a pore size of 400 nm were expected to be small enough to go into the 0.65 μm (= 600 nm) pores of the mixed cellulose ester filter (Flaten et al., 2006b). While the liposomes extruded through filters with a pore size of 800 nm were expected to be larger than 0.65 μm so they could not pass through the mixed cellulose ester filter but produce a layer on the top (Flaten et al., 2006b). The size of the liposomes was measured after extrusion to see if the desired liposome size distributions had been obtained (Section 4.2.1.4). The results from the size measurement show that the liposomes extruded through filters with a pore size of 400 nm had their size distributed around 500 nm (519 nm \pm 57 nm; 99% of the peak intensity area), indicating that the liposomes would fit into the pores of the mixed cellulose ester filter. The liposomes extruded through filters with a pore size of 800 nm had their size distributed around 700 nm (735 nm \pm 50 nm; 86% of the peak intensity area), indicating that the liposomes would produce a layer on top of the mixed cellulose ester filter.

5.1.2 Mucus-PVPA barrier integrity

The barrier integrity of the mucus-PVPA model was investigated in order to evaluate whether the fenofibrate-containing SNEDDSs dispersed in HTP medium with or without lipolysis would affect the integrity of the barriers. The integrity of the mucus-PVPA barriers was evaluated by two different methods: Measurement of the electrical resistance (ER) across the barriers immediately after lipolysis-permeation, and by measurement of the P_{app} of the hydrophilic marker calcein (Section 4.4.2). This approach has also been previously used in evaluating the mucus-PVPA barrier integrity (Falavigna et al., 2018; Falavigna et al., 2019). In barriers that are considered intact, calcein is expected to have relatively low permeability due to its hydrophilic structure. The P_{app} of calcein should not be higher than $0.06 \cdot 10^{-6}$ cm/s, as values greater than this are associated with leakage of the barrier (Falavigna et al., 2019). In the case of the electrical resistance, an electrical resistance lower than $290 \Omega \cdot \text{cm}^2$ is a sign of compromised barrier integrity (Falavigna et al., 2019). The mean values and standard deviations (SD) of the P_{app} of calcein and the electrical resistance measured during the lipolysis-permeation for each formulation with and without lipolysis are given in **Table 7**. The results show that there is a difference in barrier compatibility between the fenofibrate-containing SNEDDSs with and without lipolysis. An explanation for this could be connected to the different colloidal structures resulting from the lipolysis and/or dispersion of the SNEDDS in the HTP medium. Without lipolysis, SNEDDS display a very distinct structure, while during lipolysis different colloidal structures (mixed micelles, unilamellar and multilamellar vesicles) composed of both lipolysis products (e.g. monoglycerides and fatty acids) and components present in the lipolysis medium (e.g. bile salts and phospholipids) are formed (Michaelsen et al., 2019). Overall, the results show that in terms of calcein permeability and electrical resistance, the integrity of the mucus-PVPA barriers appeared to be maintained during the *in vitro* lipolysis-permeation experiment.

Table 7: The apparent permeability of calcein and the electrical resistance of the mucus-PVPA barriers during lipolysis-permeation experiments. Results expressed as mean \pm SD, n=18 (mucus-PVPA barriers).

	Fluorescent marker	Concentration (mM)	Permeability (10^{-6} cm/s)	Mean resistance (Ω cm²)
Super-SNEDDS solution 150% (with lipolysis)	Calcein	5	0.023 \pm 0.005	562 \pm 37
SNEDDS 75% (with lipolysis)	Calcein	5	0.027 \pm 0.001	541 \pm 5
Super-SNEDDS suspension 150% (with lipolysis)	Calcein	5	0.018 \pm 0.004	818 \pm 112
Super-SNEDDS solution 150% (without lipolysis)	Calcein	5	0.050 \pm 0.017	422 \pm 22
SNEDDS 75% (without lipolysis)	Calcein	5	0.055 \pm 0.002	373 \pm 8
Super-SNEDDS suspension 150% (without lipolysis)	Calcein	5	0.057 \pm 0.011	450 \pm 3

5.1.3 Electrical conductivity of lipolysis media

The EC of the lipolysis media listed in **Table 6** was measured to investigate if the EC amongst the different lipolysis media were similar to each other (Section 4.3.5). The EC of a solution depends on its ionic strength, which is the total ion concentration in the solution. Stability of emulsion droplets can be affected by the ionic strength of the dispersion medium (e.g. lipolysis medium) and it is therefore important to have similar EC among the lipolysis media in order to compare the resulting emulsions (Mosgaard et al., 2015). The results from the EC measurements are presented in **Table 8**, which shows that the fasted state intestinal medium (with and without calcein) has higher conductivity compared to HTP medium (with and without calcein). Additionally, the presence of calcein did not significantly influence the EC of the lipolysis media investigated. The higher EC in fasted state intestinal medium (with and without calcein) could be explained by the higher amount of NaCl in this medium, compared to the HTP medium (**Table 6**). Moreover, it has previously been stated that the high amount of Bis-Tris in the HTP medium would not contribute to altered ionic strength (Mosgaard et al., 2015). The observed difference in EC between the two lipolysis media could affect the stability of the SNEDDS emulsion, and thus have an effect on the drug solubilization capacity of the SNEDDS and on the permeation of the drug in these two different conditions.

Table 8: EC measurements of different lipolysis media. Results expressed as mean \pm SD, n=3.

	Conductivity (mS/cm)
HTP medium	8.05 \pm 0.78
HTP medium with calcein	8.88 \pm 0.73
Fasted state intestinal medium	14.08 \pm 0.46
Fasted state intestinal medium with calcein	15.35 \pm 1.52

5.2 *In vitro* lipolysis-permeation of fenofibrate-containing SNEDDS

The fenofibrate-containing SNEDDSs (i.e. Super-SNEDDS solution 150%, SNEDDS 75% and Super-SNEDDS suspension 150%) were investigated in terms of their degree of lipolysis, drug solubilization capacity and drug permeation using the combined *in vitro* lipolysis-permeation model, where the mucus-PVPA barriers were used as the *in vitro* permeation tool on top of which *in vitro* lipolysis was occurring simultaneously.

5.2.1 *In vitro* lipolysis results

The lipolysis of the fenofibrate-containing SNEDDSs was conducted at room temperature (23-25 °C) and at 37 °C to simulate physiologically relevant temperature. This was done to assess if the different temperatures would have an impact of the fenofibrate distribution during lipolysis to further consider if the setup could be used at room temperature (23-25 °C). During the *in vitro* lipolysis, the relative amount of fenofibrate in the aqueous phase and pellet phase was determined before initiation of lipolysis and during lipolysis at the time points 30 minutes and 6 hours (Section 4.4.1). The results are presented in **Figure 8**. The pH of the lipolysis medium was measured throughout the duration of the lipolysis.

For the Super-SNEDDS solution 150%, the amount of fenofibrate maintained solubilized in the aqueous phase before lipolysis (0 min) was significantly higher at 37 °C compared to room temperature (23-25 °C) (**Figure 8 (A)**). After initiation of lipolysis, a similar fenofibrate distribution was observed at both temperatures; the amount of fenofibrate in the pellet phase increased gradually after the first 30 minutes and after 6 hours of lipolysis. The pH during lipolysis of Super-SNEDDS solution 150%, dropped from approximately 6.50 to 6.48 ± 0.03 during the 6 hours of lipolysis at room temperature (23-25 °C) and the pH dropped from approximately 6.50 to 6.48 ± 0.02 during the 6 hours of lipolysis at 37 °C.

For the SNEDDS 75% almost the entire amount of fenofibrate was maintained solubilized in the aqueous phase before lipolysis and during the first 30 minutes of lipolysis at both room temperature (23-25 °C) and at 37 °C (**Figure 8 (B)**). However, after 6 hours of lipolysis the amount of fenofibrate solubilized in the aqueous phase decreased significantly at 37 °C compared to room temperature (23-25 °C). The pH during lipolysis of SNEDDS 75%, dropped from approximately 6.50 to 6.45 ± 0.03 during the 6 hours of lipolysis at room temperature (23-

25 °C) and the pH dropped from approximately 6.50 to 6.45 ± 0.02 during the 6 hours of lipolysis at 37 °C.

For the Super-SNEDDS suspension 150%, there was no significant difference between the fenofibrate distribution during lipolysis at room temperature (23-25 °C) and at 37 °C (**Figure 8** (C)). The fenofibrate was mainly located in the pellet phase before initiation of lipolysis and increased gradually throughout the lipolysis. The pH during lipolysis of Super-SNEDDS suspension 150%, dropped from approximately 6.50 to 6.47 ± 0.02 during the 6 hours of lipolysis at room temperature (23-25 °C), and the pH dropped from approximately 6.50 to 6.44 ± 0.02 during the 6 hours of lipolysis at 37 °C.

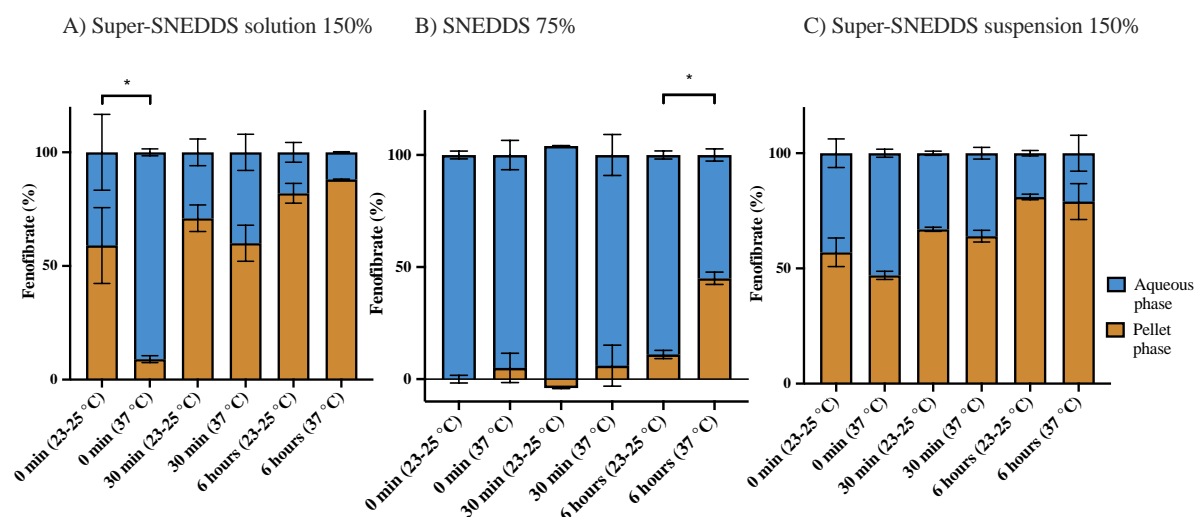


Figure 8: Fenofibrate distribution (%) in the pellet phase (brown) and the aqueous phase (blue) during lipolysis in HTP medium at room temperature (23-25 °C) and at 37 °C of Super-SNEDDS solution 150% (A), SNEDDS 75% (B) and Super-SNEDDS suspension 150% (C). Results expressed as mean \pm SD, n = 3.

The results of the pH measurements show that pH during lipolysis was maintained at satisfactory levels at both room temperature (23-25 °C) and at 37 °C, considering that the physiological pH in the intestine during fasted state is usually within the range of 6–7.5 (Larsen et al., 2011). The significant difference in amount of drug in the aqueous phase seen for the Super-SNEDDS solution 150% before lipolysis (0 min) between room temperature (23-25 °C) and 37 °C could come from the fact that the formulation only manages to keep fenofibrate

solubilized in the supersaturated state at 37 °C. However, at room temperature (23-25 °C) fenofibrate is more likely to precipitate because the solubility capacity of the formulation might be reduced (Ilie et al., 2020). A significant difference was also found for the SNEDDS 75% after 6 hours of lipolysis between room temperature (23-25 °C) and 37 °C. On the basis of these significant findings between the two temperatures, the *in vitro* lipolysis should be conducted at 37 °C for a more precise estimation of fenofibrate distribution from the three fenofibrate-containing SNEDDSs.

In the study conducted by Michaelsen and colleagues the same three fenofibrate-containing SNEDDSs were exposed to *in vitro* lipolysis, and the fenofibrate solubilization profiles were studied (Michaelsen et al., 2019). In the mentioned study, the percentage of precipitated fenofibrate during lipolysis was higher compared to the results from the present study. A possible explanation for this could be the different setups used by the two studies. More specifically, the addition of calcium differed between the two models. In the current study, calcium was added as an initial bolus at a fixed concentration (4.50 mM) at the beginning of the lipolysis experiment (static lipolysis model), whereas in the study by Michaelsen and colleagues calcium was added continuously to the lipolysis medium over the time course of *in vitro* lipolysis (dynamic lipolysis model) (Michaelsen et al., 2019). It has previously been demonstrated that the two calcium addition schemes (i.e. the static lipolysis model and the dynamic lipolysis model) affect the distribution of drugs during lipolysis of LbDDSs differently (Sassene et al., 2014).

During lipolysis of all three fenofibrate-containing SNEDDSs, the fenofibrate concentration in the lipolysis media was kept constant. However, because of the different drug loading among the formulations (**Table 3**), the Super-SNEDDS solution 150% and Super-SNEDDS suspension 150% dosing contained less SNEDDS pre-concentrate than SNEDDS 75% to achieve the predetermined fenofibrate concentration (480 µg/ml). The SNEDDS pre-concentrate consists of various lipid excipients that are hydrolyzed during lipolysis, and the lipolysis products (e.g. monoglycerides and fatty acids) together with bile salts and phospholipids can enhance the drug solubilization capacity in the lipolysis media (Michaelsen et al., 2019). The higher lipid excipient-to-drug ratio in SNEDDS 75% compared to the other two formulations could therefore explain why a difference could be observed between the solubility capacities of these SNEDDSs.

Both Super-SNEDDS solution 150% and Super-SNEDDS suspension 150% have inferior solubilization capacities (**Figure 8 (A/C)**) compared to SNEDDS 75% (**Figure 8 (B)**). Based on the assumption that only drug in solution is available for absorption, it would be expected that the SNEDDS 75% would give the best *in vivo* performance (Dahan and Hoffman, 2006). However, this is not always the case. In fact, to rely solely on *in vitro* lipolysis data on the prediction of the performance of LbDDS has shown to not correlate well with *in vivo* data (Siqueira et al., 2017; Thomas et al., 2014). An *in vitro* lipolysis setup is a closed system, which differs from the *in vivo* situation, where the surface area in the small intestine provides an absorption sink. Therefore, adding an absorption step to the *in vitro* lipolysis model would give a better estimation of drug absorption from LbDDSs, and thus correlate better with *in vivo* data (Berthelsen et al., 2019; Feeney et al., 2016).

5.2.2 *In vitro* lipolysis in the donor compartment

The lipolysis part which included the assessment of the degree of lipolysis and drug solubilization capacity took place in a lipolysis vessel where the lipolysis medium was stirred by a magnetic stirrer (Section 4.4.1). However, in the donor compartment on top of the mucus-PVPA barriers, it is not possible to have stirring devices. To assess the influence of stirring on fenofibrate distribution, lipolysis i) without stirring (Section 4.4.3.1), and ii) without stirring and with no pancreatin addition (i.e. no lipolysis occurring) (Section 4.4.3.2) was conducted for each formulation. The results are presented in **Figure 9**. The extent of overall drug solubilization during lipolysis was found to be significantly higher for the Super-SNEDDS solution 150% (**Figure 9 (A)**) and SNEDDS 75% (**Figure 9 (B)**) without stirring as compared to with stirring (**Figure 8 (A)** and **Figure 8 (B)**). However, Super-SNEDDS suspension 150% without stirring did not have a significant difference on the extent of overall drug solubilization during lipolysis. Moreover, the overall solubilization capacity of the Super-SNEDDS solution 150% (**Figure 9 (D)**) and Super-SNEDDS suspension 150% (**Figure 9 (F)**) without stirring and without lipolysis was significantly higher as compared to with without stirring and with lipolysis (**Figure 9 (A)** and **Figure 9 (C)**). However, the SNEDDS 75% lipolysis did not have a significant difference on the extent of overall drug solubilization.

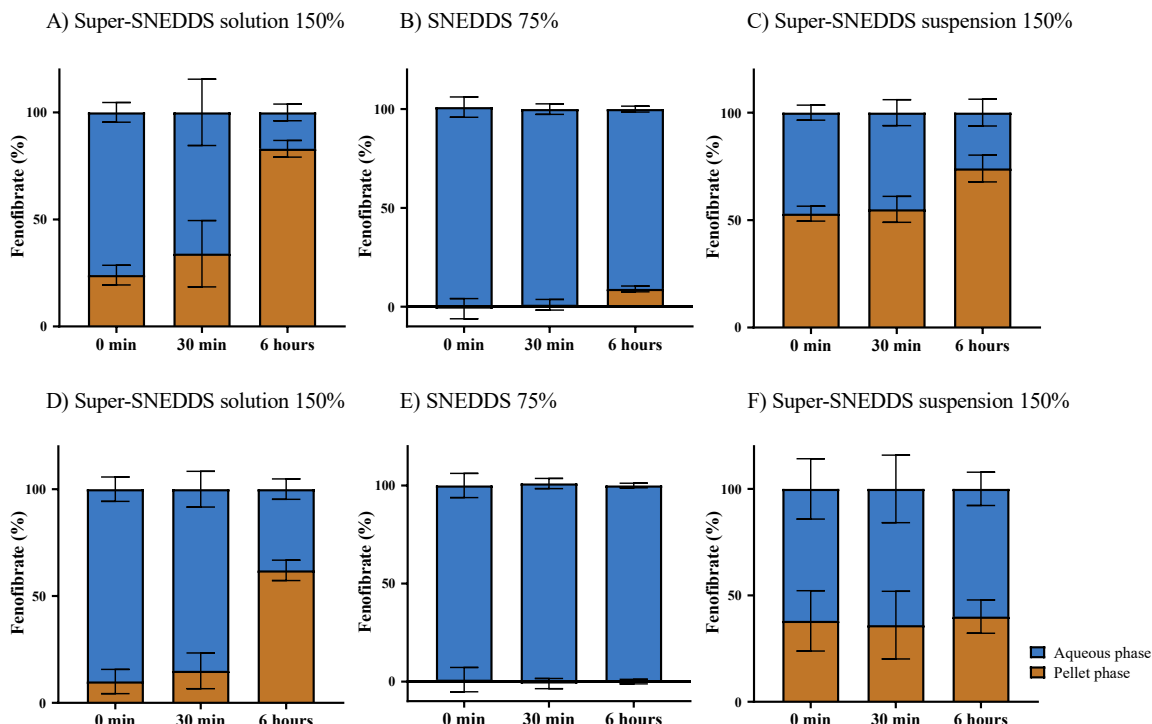


Figure 9: Fenofibrate distribution (%) in the pellet phase (brown) and the aqueous phase (blue) during lipolysis without stirring in HTP medium at 37 °C of Super-SNEDDS solution 150% with lipolysis (A), SNEDDS 75% with lipolysis (B), Super-SNEDDS suspension 150% with lipolysis (C), Super-SNEDDS solution 150% without lipolysis (D), SNEDDS 75% without lipolysis (E), and Super-SNEDDS suspension 150% without lipolysis (F). Results expressed as mean \pm SD, n = 3.

Stirring had a significant impact on fenofibrate distribution for Super-SNEDDS solution 150% and SNEDDS 75%. The reason for this could be that stirring increases the probability of collisions between pancreatic lipase and its substrates, and thus more lipolysis is facilitated (Kadia et al., 2014). Without stirring, there are less collisions and thus a lower extent of lipolysis is taking place and results in lower fenofibrate precipitation. The significant increase in overall drug solubility observed for Super-SNEDDS solution 150% and Super-SNEDDS suspension 150% without lipolysis (**Figure 9 (D)** and **Figure 9 (F)**) compared to the same formulations with lipolysis (**Figure 9 (A)** and **Figure 9 (C)**) is most likely related to the absence of lipase activity, which has previously shown to have an impact on drug precipitation (Sassene et al., 2014).

5.2.3 *In vitro* permeation results

The rate and extent of fenofibrate permeation from the three fenofibrate-containing SNEDDSs (i.e. Super-SNEDDS solution 150%, SNEDDS 75% and Super-SNEDDS suspension 150%) with and without lipolysis was assessed with the use of the mucus-PVPA barriers. The experiment was conducted with and without lipolysis to see if this process had an impact on permeation (Section 4.4.1). The results are presented in **Figure 10** as cumulative amount of fenofibrate permeated over time at 37 °C. From these results, the Super-SNEDDS solution 150% display a significantly higher permeation profile than SNEDDS 75% both with and without lipolysis, whereas the permeation profile of Super-SNEDDS suspension 150% is not significantly different than Super-SNEDDS solution 150% or SNEDDS 75% with and without lipolysis. Although not significant, the presence of lipolysis appears to affect the permeation profile of Super-SNEDDS suspension 150%. For this reason, the overall ranking of the formulations appears to be different depending on whether or not lipolysis is present. From **Figure 10 (A)** (without lipolysis) the rank order of the formulations is as follows: Super-SNEDDS solution 150% > Super-SNEDDS suspension 150% > SNEDDS 75%. While from **Figure 10 (B)** (with lipolysis) the ranking is; Super-SNEDDS solution 150% > SNEDDS 75% = Super-SNEDDS suspension 150%. The permeation results were also used to plot the area under the curve (AUC), calculated from the cumulative amount of fenofibrate permeated (**Figure 11**). In terms of AUC data, none of the fenofibrate-containing SNEDDSs did change significantly with or without lipolysis. Nevertheless, the presence or absence of lipolysis appeared to be the main contributor to the different rankings of the formulations.

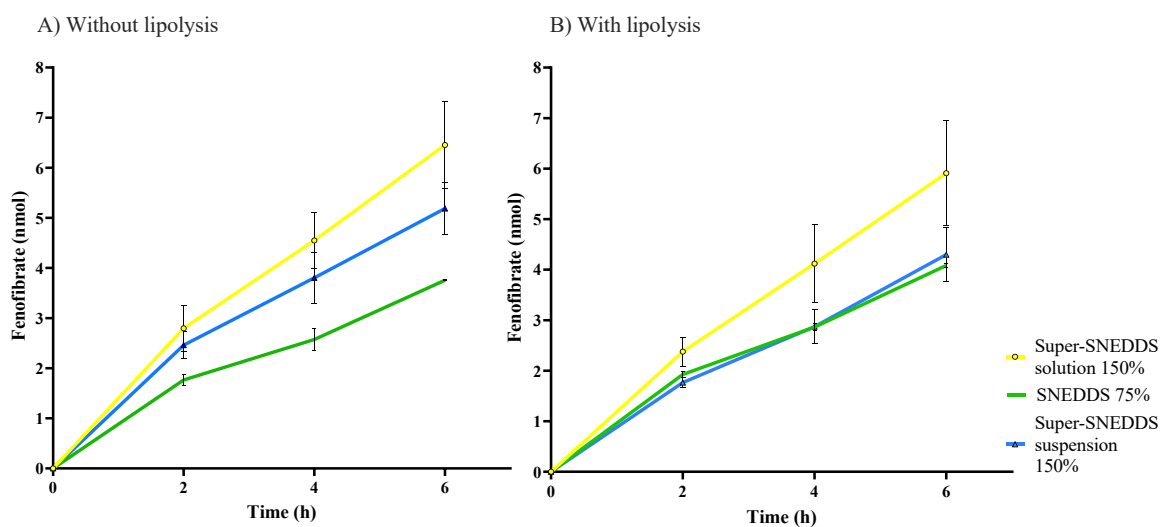


Figure 10: Cumulative amount of fenofibrate permeated across mucus-PVPA barriers A) without lipolysis and B) with lipolysis. (Results expressed as mean \pm SD; n=18 (mucus-PVPA barriers)).

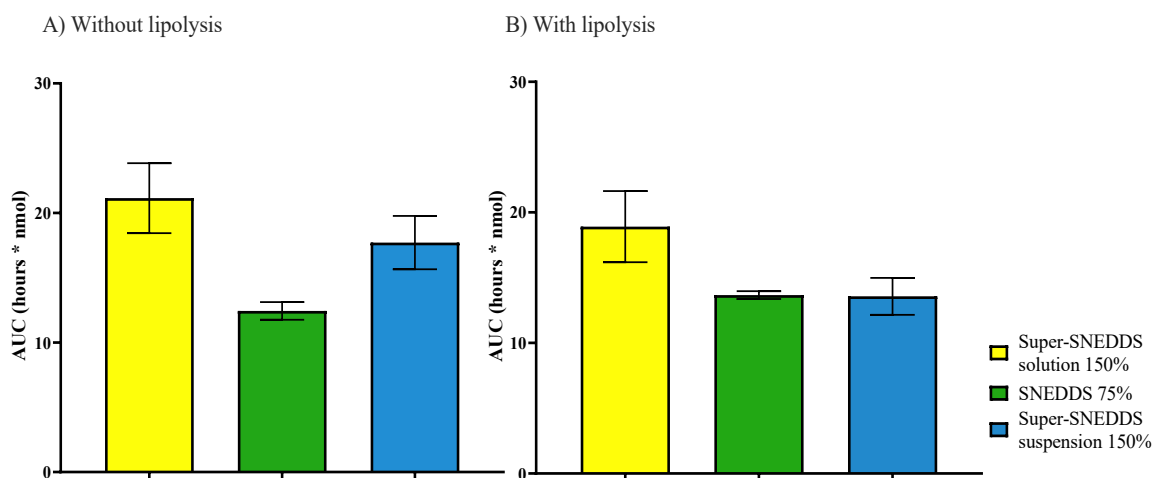


Figure 11: AUC calculated from cumulative amount of fenofibrate permeated across mucus-PVPA barriers A) without lipolysis and B) with lipolysis. (Results expressed as mean \pm SD; n=18 (mucus-PVPA barriers)).

An *in vitro* study conducted by Falavigna and colleagues used the same fenofibrate-containing SNEDDSs as the present study, however, in contrast to the present study the ranking of the formulations in terms of extent and rate of fenofibrate permeation appeared to be unaffected by the presence or absence of lipolysis (Falavigna et al., 2020a). The present study has the same ranking of the formulations after lipolysis as Falavigna and colleagues, whereas without lipolysis, an increase in *in vitro* AUC is observed for the Super-SNEDDS suspension 150%, resulting in a rearrangement of the rankings of the formulations. A similar result was also observed in the study by Michaelsen and colleagues, where the inhibition of lipolysis by addition of the lipase inhibitor orlistat resulted in an increased *in vivo* AUC in rats for the same Super-SNEDDS suspension 150% (Michaelsen et al., 2019). As an explanation for this, it was suggested that the addition of a lipase inhibitor would prolong the absorption phase of fenofibrate, thus leading to higher AUC (Michaelsen et al., 2019).

The results from the *in vitro* lipolysis showed that the SNEDDS 75% was the formulation with the highest amount of fenofibrate solubilized, and thus expected to have the highest amount of fenofibrate permeating. This was however not what was observed after *in vitro* permeation. The formulation that presented the best permeation profile for fenofibrate during lipolysis was the Super-SNEDDS solution 150%. This finding highlights the fact that the amount of drug solubilized does not necessarily reflect the amount of drug absorbed. Actually, the drug that is solubilized in the aqueous phase of the lipolysis medium during *in vitro* lipolysis does not only consist of free drug, but also drug solubilized in colloidal structures (e.g. mixed micelles, unilamellar and multilamellar vesicles) formed by lipolysis products and endogenous components (Berthelsen et al., 2019). Only the drug free in solution is available for absorption; however, since it is not possible to distinguish between these two types of drug solubilization in the *in vitro* lipolysis model, it is highly likely that the model overestimates how much drug is available for absorption compared to *in vivo*.

5.2.4 *In vivo-in vitro* correlation

The *in vitro-in vivo* correlation was investigated by plotting the AUC obtained from the present study with *in vivo* data obtained from a pharmacokinetic study in rats conducted by Michaelsen and colleagues (Michaelsen et al., 2019). In the *in vivo* study, the same fenofibrate-containing SNEDDSs were used (Super-SNEDDS solution 150%, SNEDDS 75% and Super-SNEDDS suspension 150%). In addition, the lipase inhibitor orlistat was added to the SNEDDS to assess the influence of lipolysis, resulting in an additional *in vivo* setup comprising Super-SNEDDS solution 150% with orlistat, SNEDDS 75% with orlistat and Super-SNEDDS suspension 150% with orlistat. All of the *in vitro* and *in vivo* data used for the *in vitro-in vivo* correlations are presented in **Table 9**. The Pearson correlation coefficient was used as a measure of linear correlation between the different *in vitro* and *in vivo* data sets.

Table 9: *In vitro* and *in vivo* data used for *in vitro-in vivo* correlation. Results expressed as mean \pm SD, n=18 (mucus-PVPA barriers).

	Super-SNEDDS solution 150%	SNEDDS 75%	Super-SNEDDS suspension 150%
AUC _{in vitro} (h·% in aqueous phase)	177.8 \pm 21.5	455.9 \pm 25.3	179.9 \pm 22.4
AUC _{in vitro} (h·nmol) no lipolysis	21.1 \pm 2.7	12.4 \pm 0.7	17.7 \pm 2.1
AUC _{in vitro} (h·nmol) lipolysis	18.9 \pm 2.7	13.6 \pm 0.3	13.6 \pm 1.4
AUC _{in vivo} (h· μ l/ml)	148.0 \pm 47.5	88.3 \pm 20.9	58.1 \pm 16.9
AUC _{in vivo} (h· μ l/ml) with orlistat	136.9 \pm 27.5	66.3 \pm 14.9	108.9 \pm 39.5

First, *in vitro* lipolysis data from the present study (AUC_{in vitro} (h·% in aqueous phase)) was plotted with *in vivo* absorption data (AUC_{in vivo} (h· μ l/ml)) (**Figure 12**), resulting in a poor correlation ($R^2 = 0.0371$). The poor *in vitro-in vivo* correlation highlights the fact that the *in vitro* lipolysis models are not reliable to predict the *in vivo* performance of the three fenofibrate-containing SNEDDSs tested in the present study.

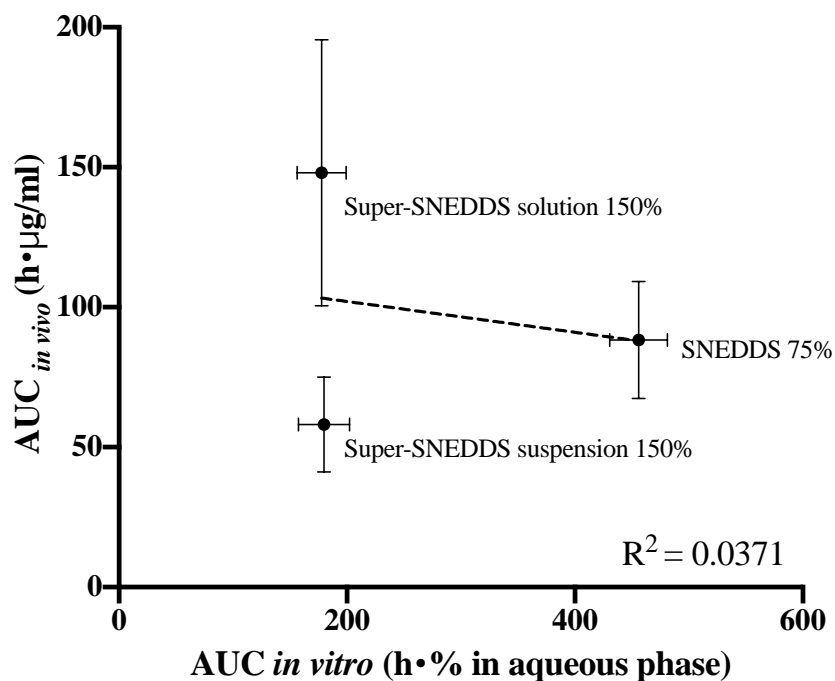


Figure 12: Linear relationship between the area under the plasma concentration-time curves ($AUC_{in vivo}$) and the area under the solubilization-time curves $AUC_{in vitro}$ (h·% in aqueous phase).

Secondly, $AUC_{in vivo}$ with orlistat was plotted against $AUC_{in vitro}$ resulting from the permeation of fenofibrate without lipolysis (**Figure 13 (A)**) to assess *in vitro-in vivo* correlation in the absence of lipolysis. Further, the $AUC_{in vivo}$ (absence of orlistat/no lipolysis inhibitor) was plotted against $AUC_{in vitro}$ resulting from the drug permeation with lipolysis (**Figure 13 (B)**) to assess *in vitro-in vivo* correlation when lipolysis was occurring. In **Figure 13 (A)** it can be observed that the correlation between *in vitro* data in the absence of lipolysis and *in vivo* data after co-administration of orlistat was excellent ($R^2 = 1$), whereas the presence of lipolysis led to a lower, but still acceptable, correlation (**Figure 13 (B)**; $R^2 = 0.9003$). The *in vitro-in vivo* correlations obtained with the combined lipolysis-permeation model, as compared to the *in vitro* lipolysis model, strongly indicate that the combination of *in vitro* lipolysis with an absorption step gives a better prediction of the *in vivo* absorption of fenofibrate from SNEDDSs.

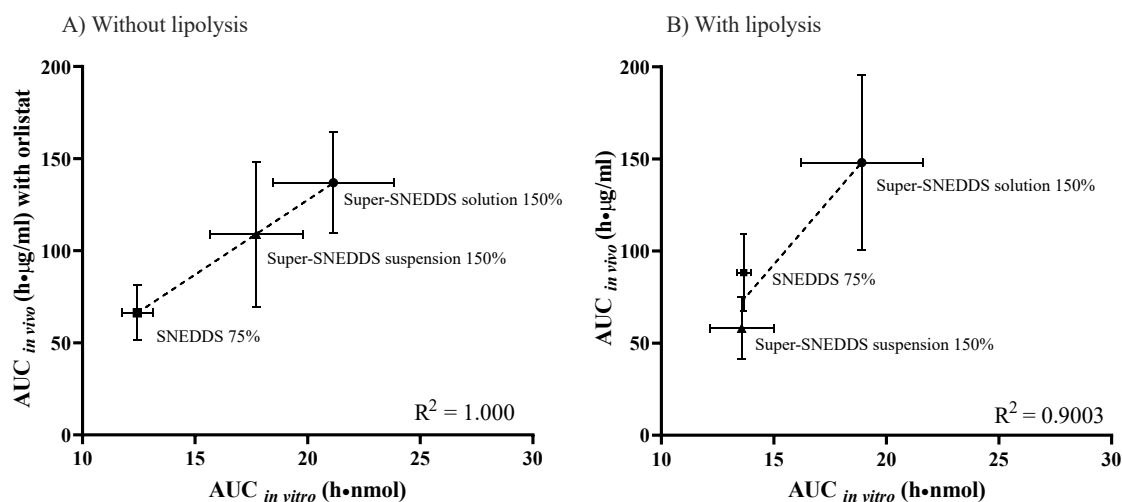


Figure 13: Linear relationship between the *in vivo* data and the *in vitro* data A) without lipolysis and B) with lipolysis.

Recently, several attempts have been made in order to combine *in vitro* lipolysis with a absorption step (Alskär et al., 2019; Bibi et al., 2017; Dahan and Hoffman, 2007; Falavigna et al., 2020a; Keemink and Bergström, 2018; Keemink et al., 2019; Klitgaard et al., 2019). The study by Falavigna and colleagues combined the pH-stat lipolysis model with the mucus-PVPA permeation assay, which led to a good *in vitro-in vivo* correlation for fenofibrate-containing SNEDDSs (Falavigna et al., 2020a). To our knowledge, the present study and the study by Falavigna et al., 2020a are the only studies that have included the mucus-PVPA as the absorption step in a lipolysis-permeation model. Other lipolysis-permeation studies that have used different *in vitro* permeation assays as their absorption step, have not included a mucus layer in the model. The mucus layer is the first physical barrier the drug has to encounter in the GI tract, and the mucus has proven to affect the permeability of many drugs (Murgia et al., 2018). Therefore, by incorporating a mucus layer into the *in vitro* lipolysis-permeation model, it will be possible to mimic the intestinal mucosa barrier more closely (Falavigna et al., 2018).

The results obtained in the presented work have showed that, by the use of the HTP *in vitro* combined lipolysis-permeation model, we were able to successfully combine lipolysis with permeation for the assessment of fenofibrate absorption from SNEDDSs. What makes the presented HTP *in vitro* combined lipolysis-permeation model unique compared to other lipolysis-permeation models is its HTP applicability. The HTP lipolysis model used in combination with the mucus-PVPA model in the present study, does not require any NaOH

titration during lipolysis. This simplifies the setup substantially and makes rapid screening of LbDDSs more obtainable, which is very desirable in formulation development (Mosgaard et al., 2015). In addition, the presented model showed great potential for further use to evaluate the performance of LbDDSs based on its remarkable ability to predict the *in vivo* absorption of fenofibrate from SNEDDSs.

5.3 Comparison between the HTP medium and fasted state intestinal medium

The differences in the results from the present study compared to the study by Falavigna et al., 2020a can be justified by the different experimental setups of the *in vitro* lipolysis applied in the two studies. However, we wanted to investigate in more detail how the setups might cause these differences in the results. Elements like the mucus-PVPA, calcium addition (static lipolysis model), the fenofibrate-containing SNEDDSs and the calcein concentration in the lipolysis media was kept the same in the two models, so no further investigation was done for these elements as they are unlikely to be the driving force for the difference between the mentioned results. Thus, the focus was put on finding differences between the HTP medium and the fasted state intestinal medium according to droplet size of the fenofibrate-containing SNEDDSs and the appearance of the precipitate.

5.3.1 Droplet size measurement

Droplet size measurement of drug free SNEDDS was carried out to assess if i) emulsification of the SNEDDS took place upon dispersion in the two lipolysis media (i.e. HTP medium with calcein and fasted state intestinal medium with calcein), and ii) if there were any size distribution differences of resulting emulsions. The size measurements were done with a Zetasizer (Section 4.3.6) and the results are presented in **Table 10**. Some very large particles (> 4000 nm) were present during dispersion of SNEDDS in both lipolysis media, but were believed to be dust particles and thus neglected, as previously discussed (Mosgaard et al., 2015). The SNEDDS dispersed in the fasted state intestinal medium with calcein appeared to be monodispersed with the major size distribution at 51 ± 3 nm, which accounted for 96% of the global peak intensity areas, and the polydispersity index (PDI) was found to be 0.20 ± 0.04 . The SNEDDS dispersed in the HTP medium with calcein had a bimodal size distribution with a peak at 58 nm and a second peak at 395 nm which accounted for 68% and 29% of the peak

intensity areas and the PDI was found to be 0.44 ± 0.04 . Overall, we can conclude that the emulsification of the SNEDDS did take place as the size measurements were able to detect droplets in both lipolysis media. However, resulting emulsions had a different appearance in the case of HTP medium compared to fasted state intestinal medium. The size of the emulsion droplets is of importance because the lipolysis rate is surface area dependent (Salvia-Trujillo et al., 2013). For this reason, differences in droplet size could affect the lipolysis process. This could be a possible contributor to the reason why the present results were different from the ones from Falavigna and colleagues (Falavigna et al., 2020a).

Table 10: Size distribution by intensity of the droplets present after dispersion of SNEDDS in the two lipolysis media. Results expressed as mean \pm SD, n=6.

Lipolysis medium	PDI	Peak 1 (nm) [%]	Peak 2 (nm) [%]	Peak 3 (nm) [%]
HTP medium with calcein	0.44 ± 0.04	58 ± 5 [68 \pm 2]	395 ± 49 [29 \pm 2]	5074 ± 192 [3 \pm 1]
Fasted state intestinal medium with calcein	0.20 ± 0.04	51 ± 3 [96 \pm 2]	4152 ± 560 [4 \pm 2]	-


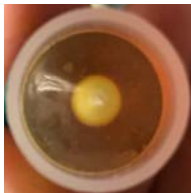

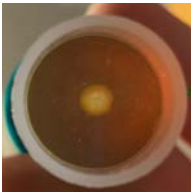

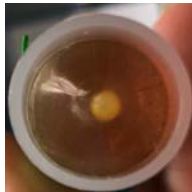

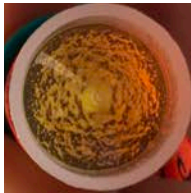

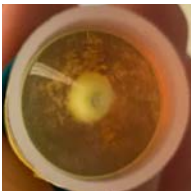
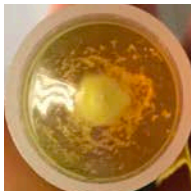

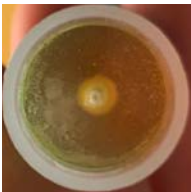


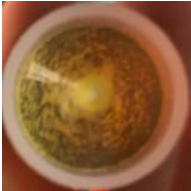
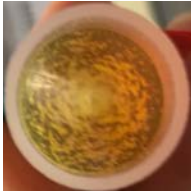
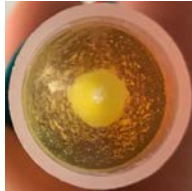
5.3.2 *In vitro* lipolysis pellet analysis

5.3.2.1 Macroscopic analysis

Pictures were taken of the pellet formed from the fenofibrate-containing SNEDDSs in HTP medium with calcein or in fasted state intestinal medium with calcein. In order to account for the lipolysis conditions occurring on top of the mucus-PVPA barriers no stirring were performed in any of the experiments. The pictures are presented in **Table 11** and show the pellet either with or without lipolysis. Without lipolysis, a distinct difference in the pellet formation among the different formulations could be observed independent of lipolysis media. The pellet from both Super-SNEDDS solution 150% and SNEDDS 75% accumulates in the bottom center of the test tube in a circular arrangement. What mainly separate the pellet formations between the two formulations is that the SNEDDS 75% has a smaller quantity of pellet. The Super-SNEDDS suspension 150% also show some accumulation of pellet in the center but has additionally pellet spread out all over the bottom of the test tube. With lipolysis, there was not a distinct difference in the pellet formation among the formulations in the fasted state intestinal medium. However, for the HTP medium there was a difference between the SNEDDS 75% pellet compared to Super-SNEDDS solution 150% and Super-SNEDDS suspension 150%, as they appeared to be precipitating in different patterns. The Super-SNEDDS solution 150% and the Super-SNEDDS suspension has their pellet mainly accumulated in the bottom center of the test tube. However, the pellet from SNEDDS 75% did not accumulate in the bottom center of the test tube in the same extent as it did for the other two formulations.

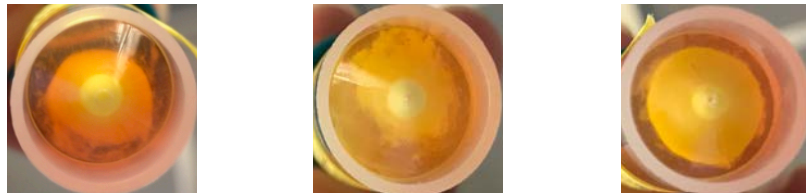
Even though insightful in terms of the characterization of the pellet, the pictures depicted in **Table 11** are not accurate enough to be able to draw any conclusions from them. However, they indicated that a difference in the pellet formation using either HTP medium or fasted state intestinal medium could be observed, and this could be part of the reason for the difference between the results presented in this study compared to the ones from Falavigna and colleagues (Falavigna et al., 2020a).

Table 11: Pictures of pellet formed from the three fenofibrate-containing SNEDDSs during lipolysis without stirring in HTP medium or in fasted state intestinal medium with and without lipolysis.

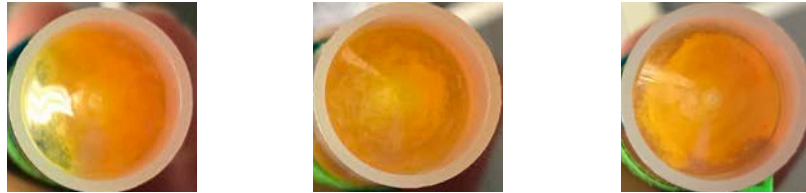
Formulations	1. Replicate	2. Replicate	3. Replicate
HTP medium - without lipolysis			
Super-SNEDDS solution 150%			
SNEDDS 75%			
Super-SNEDDS suspension 150%			
Fasted state intestinal medium - without lipolysis			
Super-SNEDDS solution 150%			
SNEDDS 75%			
Super-SNEDDS suspension 150%			

HTP medium – with lipolysis

Super-SNEDDS
solution 150%



SNEDDS 75%



Super-SNEDDS
suspension 150%



Fasted state intestinal medium – with lipolysis

Super-SNEDDS
solution 150%



SNEDDS 75%



Super-SNEDDS
suspension 150%


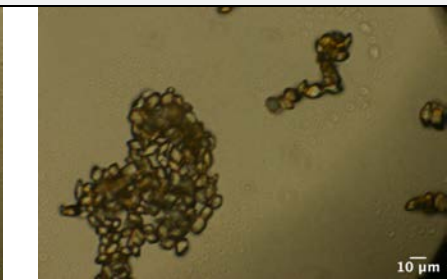

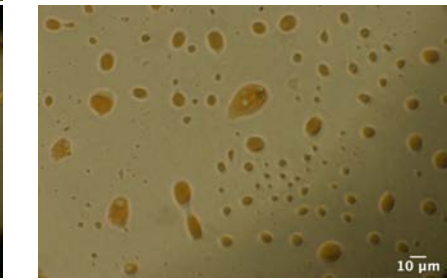
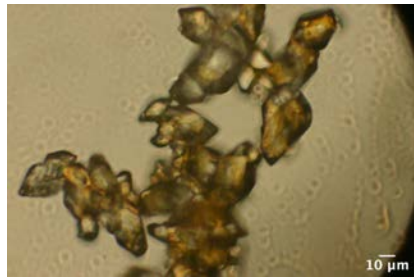
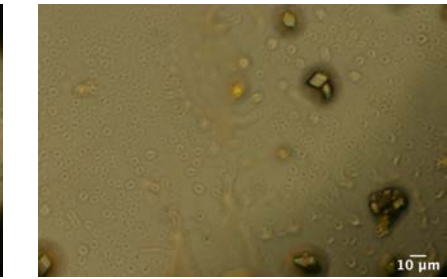
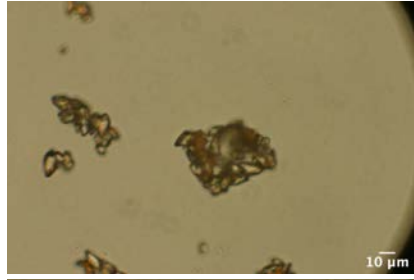
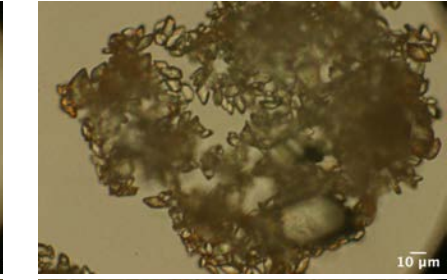
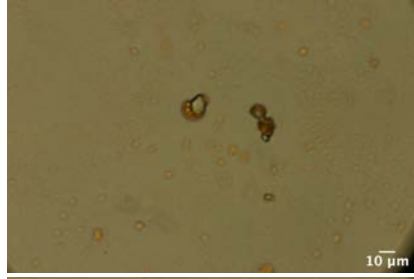
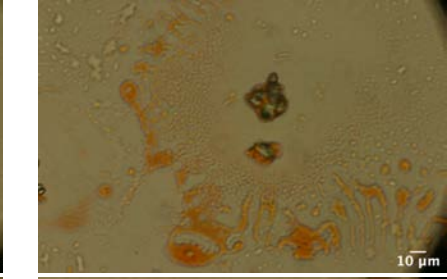
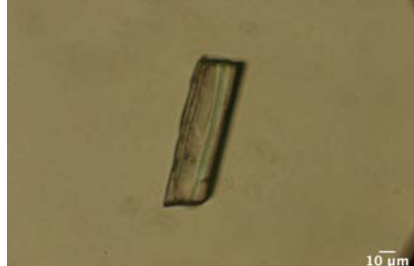



5.3.2.2 Microscopic analysis

Microscopic analysis by polarized light microscopy was conducted to analyze the pellet resulting from the three fenofibrate-containing SNEDDSs in HTP medium with calcein or in fasted state intestinal medium with calcein (Section 4.4.5). In order to account for the lipolysis conditions occurring on top of the mucus-PVPA barriers no stirring were performed in any of the experiments. The pictures are presented in **Table 12** and show the fenofibrate pellet either with or without lipolysis. Fenofibrate has previously shown to precipitate in a crystalline solid state during lipid digestion from LbDDSs (Thomas et al., 2014; Williams et al., 2013). However, the morphology of the crystals has previously shown to be dependent on the specific formulation (Michaelsen et al., 2019). We wanted to further investigate if the morphology also could differ in the presence of different lipolysis media (i.e. HTP medium with calcein and fasted state intestinal medium with calcein), and whether or not lipolysis had an impact on the crystal morphology.

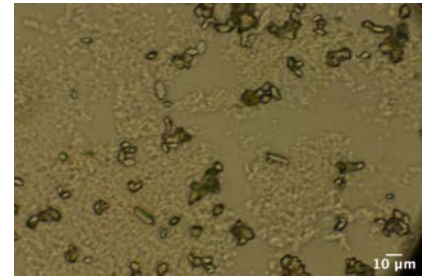
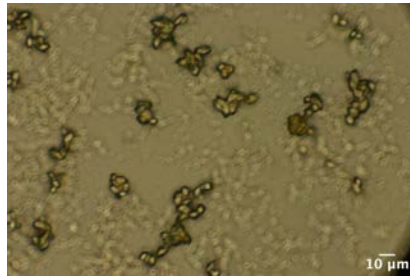
In agreement with the study by Michaelsen and colleagues, the pictures in **Table 12** show that the morphology of the fenofibrate crystals are dependent on the specific formulation (Michaelsen et al., 2019). For the Super-SNEDDS suspension 150%, in the absence of lipolysis, the crystals look smaller in the HTP medium compared to the crystals in fasted state intestinal medium (**Table 12**). Small crystals usually dissolves more quickly than larger ones because of the increased surface areas (Noyes and Whitney, 1897). This could explain why the Super-SNEDDS suspension 150% without lipolysis exhibited a better performance in terms of absorption in the present setup compared to the setup by Falavigna and colleagues (Falavigna et al., 2020a). For the crystals from each formulation with lipolysis present, no distinct difference was observed between the two lipolysis media. This is to be expected because of the similar ranking of the fenofibrate-containing SNEDDSs with lipolysis from this setup and the setup by Falavigna and colleagues (Falavigna et al., 2020a).

Table 12: Pictures from polarized light microscopy of fenofibrate crystals (scale bar 10 μm).

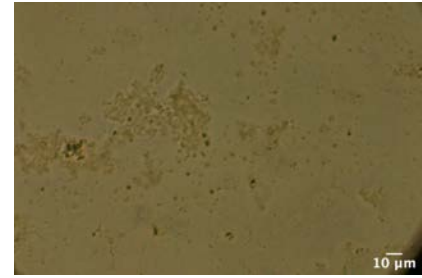
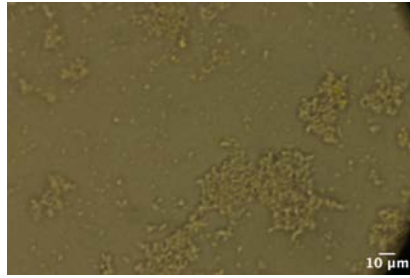
Formulations	HTP medium -without lipolysis	
Super-SNEDDS solution 150%		
SNEDDS 75%		
Super-SNEDDS suspension 150%		
Fasted state intestinal medium – without lipolysis		
Super-SNEDDS solution 150%		
SNEDDS 75%		
Super-SNEDDS suspension 150%		

HTP medium – with lipolysis

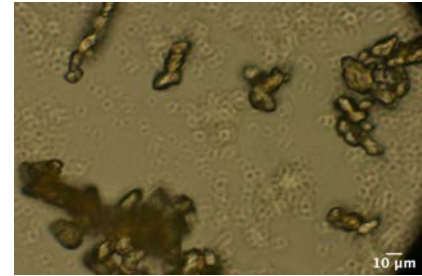
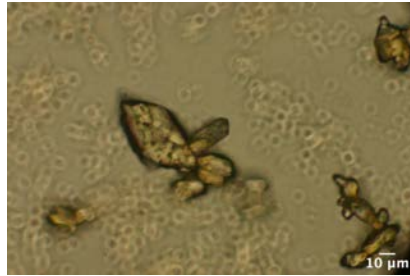
Super-SNEDDS
solution 150%



SNEDDS 75%

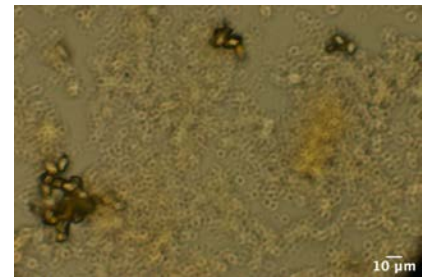
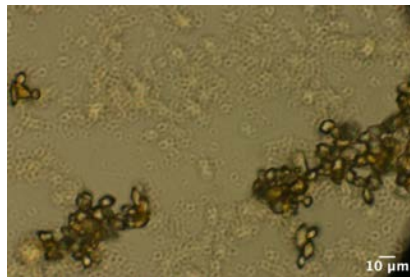


Super-SNEDDS
suspension 150%

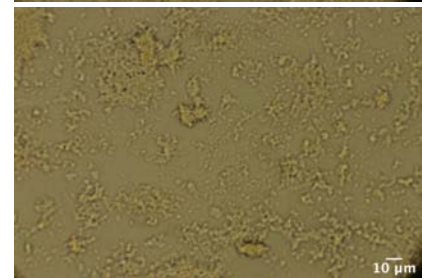
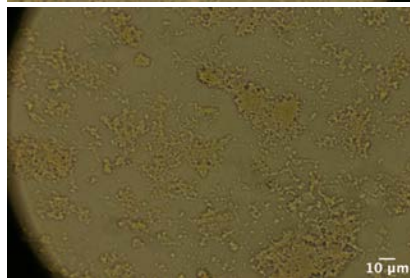


Fasted state intestinal medium – with lipolysis

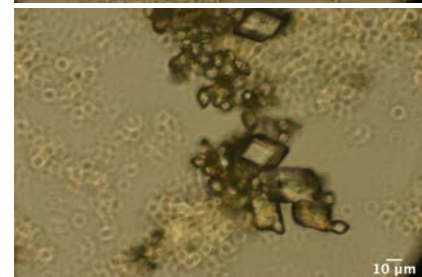
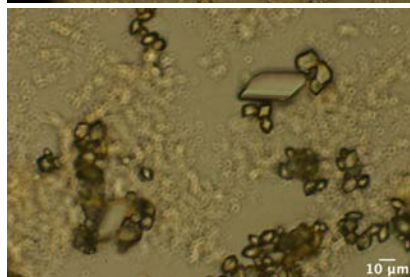
Super-SNEDDS
solution 150%



SNEDDS 75%



Super-SNEDDS
suspension 150%



The difference in the emulsion droplet size distributions and pellet appearance as well as the permeability results obtained in the present study compared to the ones from Falavigna et al., 2020a could be traced back to the difference in conductivity between the two lipolysis media utilized in the two studies, which could thus affect the stability of the emulsions and the droplet size of the SNEDDSs, and which can thus have an effect on the precipitation of the drug. However, more in depth testing needs to be done in order to conclude which driving mechanism is behind the differences between the present study compared to the one conducted by Falavigna et al., 2020a.

6 CONCLUSION

In the presented work, a new combined HTP *in vitro* lipolysis-permeation model was developed, where the mucus-PVPA barriers comprising biosimilar mucus were used as the permeation barriers and *in vitro* lipolysis was occurring in their donor compartment during the experiment. The model was validated and tested for its ability to predict the *in vivo* performance of three fenofibrate-containing SNEDDSs (i.e. Super-SNEDDS solution 150%, SNEDDS 75% and SNEDDS suspension 150%), for their degree of lipolysis, drug solubilization capacity and drug permeation. For the *in vitro-in vivo* assessment, the results obtained from the permeation data in the present study correlated with previously published *in vivo* data for the same fenofibrate-containing SNEDDSs.

The three fenofibrate-containing SNEDDSs had different drug solubilization capacities during *in vitro* lipolysis and showed a very poor *in vitro-in vivo* correlation ($R^2 = 0.03$) when compared to *in vivo* absorption data on rats. On the other hand, a great *in vitro-in vivo* correlation ($R^2 = >0.9$) was attained by plotting the *in vitro* data when the fenofibrate-containing SNEDDSs were exposed to simultaneous lipolysis and permeation by the use of the combined HTP *in vitro* lipolysis-permeation model.

At this stage, the results indicate that the presented *in vitro* model has great potential in evaluating *in vivo* performance of LbDDSs, however further testing needs to be carried out to establish the models full potential.

7 FUTURE PERSPECTIVES

The HTP lipolysis-permeation *in vitro* model employing the mucus-PVPA barriers has shown a great potential in the prediction of the *in vivo* performance of LbDDSs. To our knowledge this model is the first of its kind but has only been tested for long chain fenofibrate-containing SNEDDSs. The next appropriate step would be to assess the *in vivo* performance of different types of LbDDSs as well as drugs to widen and validate the model's ability to predict their *in vivo* performance.

8 REFERENCE LIST

- Alshamsan, A., et al. 2018. Role of alternative lipid excipients in the design of self-nanoemulsifying formulations for fenofibrate: Characterization, dispersion, digestion and gut permeation studies. *Frontiers in Pharmacology*, 9, 1219.
- Alskär, L. C., et al. 2019. Effect of lipids on absorption of carvedilol in dogs: Is coadministration of lipids as efficient as a lipid-based formulation? *Journal of Controlled Release*, 304, 90-100.
- Amidon, G., et al. 1995. A theoretical basis for a biopharmaceutic drug classification: The correlation of in vitro drug product dissolution and in vivo bioavailability. *An Official Journal of the American Association of Pharmaceutical Scientists*, 12, 413-420.
- Anby, M. U., et al. 2012. Lipid digestion as a trigger for supersaturation: Evaluation of the impact of supersaturation stabilization on the in vitro and in vivo performance of self-emulsifying drug delivery systems. *Molecular Pharmaceutics*, 9, 2063-2079.
- Armand, M. 2007. Lipases and lipolysis in the human digestive tract: Where do we stand? *Current Opinion in Clinical Nutrition and Metabolic Care*, 10, 156-164.
- Artursson, P., et al. 2001. Caco-2 monolayers in experimental and theoretical predictions of drug transport. *Advanced Drug Delivery Reviews*, 46, 27-43.
- Bannow, J., et al. 2020. Improving the drug load and in vitro performance of supersaturated self-nanoemulsifying drug delivery systems (super-SNEDDS) using polymeric precipitation inhibitors. *International Journal of Pharmaceutics*, 575, 118960.
- Berben, P., et al. 2018a. Drug permeability profiling using cell-free permeation tools: Overview and applications. *European Journal of Pharmaceutical Sciences*, 119, 219-233.
- Berben, P., et al. 2018b. Assessment of passive intestinal permeability using an artificial membrane insert system. *Journal of Pharmaceutical Sciences*, 107, 250-256.
- Bergström, C., et al. 2014. Early pharmaceutical profiling to predict oral drug absorption: Current status and unmet needs. *European Journal of Pharmaceutical Sciences*, 57, 173-199.
- Berthelsen, R., et al. 2019. In vitro digestion models to evaluate lipid based drug delivery systems; present status and current trends. *Advanced Drug Delivery Reviews*, 142, 35-49.
- Bibi, H. A., et al. 2017. Simultaneous lipolysis/permeation in vitro model, for the estimation of bioavailability of lipid based drug delivery systems. *European Journal of Pharmaceutics and Biopharmaceutics*, 117, 300-307.
- Billat, P.-A., et al. 2017. Models for drug absorption from the small intestine: where are we and where are we going? *Drug Discovery Today*, 22, 761-775.
- Boegh, M., et al. 2014. Property profiling of biosimilar mucus in a novel mucus-containing in vitro model for assessment of intestinal drug absorption. *European Journal of Pharmaceutics and Biopharmaceutics*, 87, 227-235.
- Boegh, M. and Nielsen, H. M. 2015. Mucus as a barrier to drug delivery – Understanding and mimicking the barrier properties. *Basic & Clinical Pharmacology & Toxicology*, 116, 179-186.
- Boyd, B. J., et al. 2019. Successful oral delivery of poorly water-soluble drugs both depends on the intraluminal behavior of drugs and of appropriate advanced drug delivery systems. *European Journal of Pharmaceutical Sciences*, 137, 104967.
- Butler, J., et al. 2019. In vitro models for the prediction of in vivo performance of oral dosage forms: Recent progress from partnership through the IMI OrBiTo collaboration. *European Journal of Pharmaceutics and Biopharmaceutics*, 136, 70-83.

- Crum, M., et al. 2016. A new in vitro lipid digestion – in vivo absorption model to evaluate the mechanisms of drug absorption from lipid-based formulations. *An Official Journal of the American Association of Pharmaceutical Scientists*, 33, 970-982.
- Dahan, A. and Hoffman, A. 2006. Use of a dynamic in vitro lipolysis model to rationalize oral formulation development for poor water soluble drugs: Correlation with in vivo data and the relationship to intra-enterocyte processes in rats. *An Official Journal of the American Association of Pharmaceutical Scientists*, 23, 2165-2174.
- Dahan, A. and Hoffman, A. 2007. The effect of different lipid based formulations on the oral absorption of lipophilic drugs: The ability of in vitro lipolysis and consecutive ex vivo intestinal permeability data to predict in vivo bioavailability in rats. *European Journal of Pharmaceutics and Biopharmaceutics*, 67, 96-105.
- Di Cagno, M., et al. 2015. New biomimetic barrier Permeapad™ for efficient investigation of passive permeability of drugs. *European Journal of Pharmaceutical Sciences*, 73, 29-34.
- Dickinson, P., et al. 2012. An investigation into the utility of a multi-compartmental, dynamic, system of the upper gastrointestinal tract to support formulation development and establish bioequivalence of poorly soluble drugs. *An Official Journal of the American Association of Pharmaceutical Scientists*, 14, 196-205.
- Falavigna, M., et al. 2020a. Novel in vitro model able to correctly predict in vivo absorption of drugs in lipid-based drug delivery systems: Combining in vitro lipolysis with the mucus-PVPA in vitro permeability model. Article in preparation.
- Falavigna, M., et al. 2018. Mucus-PVPA (mucus phospholipid vesicle-based permeation assay): An artificial permeability tool for drug screening and formulation development. *International Journal of Pharmaceutics*, 537, 213-222.
- Falavigna, M., et al. 2019. Mimicking regional and fasted/fed state conditions in the intestine with the mucus-PVPA in vitro model: The impact of pH and simulated intestinal fluids on drug permeability. *European Journal of Pharmaceutical Sciences*, 132, 44-54.
- Falavigna, M., et al. 2020b. Impact of mucin on drug diffusion: Development of a straightforward in vitro method for the determination of drug diffusivity in the presence of mucin. *Pharmaceutics*, 12, 168.
- FDA 2017. Waiver of in vivo bioavailability and bioequivalence studies for immediate-release solid oral dosage forms based on a biopharmaceutics classification system; guidance for industry; availability. *The Federal Register*, 82, 61011.
- Feeney, O. M., et al. 2016. 50 years of oral lipid-based formulations: Provenance, progress and future perspectives. *Advanced Drug Delivery Reviews*, 101, 167-194.
- Flaten, G. E. 2007. *The phospholipid vesicle-based barrier : a novel method for passive drug permeability screening (PhD thesis)*. University of Tromsø.
- Flaten, G. E., et al. 2006a. Drug permeability across a phospholipid vesicle-based barrier. *European Journal of Pharmaceutical Sciences*, 28, 336-343.
- Flaten, G. E., et al. 2006b. Drug permeability across a phospholipid vesicle based barrier: A novel approach for studying passive diffusion. *European Journal of Pharmaceutical Sciences*, 27, 80-90.
- Flaten, G. E., et al. 2008. Drug permeability across a phospholipid vesicle-based barrier: 4. The effect of tensides, co-solvent and pH changes on barrier integrity and on drug permeability. *European Journal of Pharmaceutical Sciences*, 34, 173-180.
- Flaten, G. E., et al. 2007. Drug permeability across a phospholipid vesicle based barrier: 3. Characterization of drug–membrane interactions and the effect of agitation on the barrier integrity and on the permeability. *European Journal of Pharmaceutical Sciences*, 30, 324-332.

- Griffin, B. T., et al. 2014. Comparison of in vitro tests at various levels of complexity for the prediction of in vivo performance of lipid-based formulations: Case studies with fenofibrate. *European Journal of Pharmaceutics and Biopharmaceutics*, 86, 427-437.
- Heshmati, N., et al. 2013. Enhancement of oral bioavailability of E804 by self-nanoemulsifying drug delivery system (SNEDDS) in rats. *Journal of Pharmaceutical Sciences*, 102, 3792-3799.
- Holm, R., et al. 2013. Bile salts and their importance for drug absorption. *International Journal of Pharmaceutics*, 453, 44-55.
- Homayun, B., et al. 2019. Challenges and recent progress in oral drug delivery systems for biopharmaceuticals. *Pharmaceutics*, 11, 129.
- Ilie, A.-R., et al. 2020. Supersaturated lipid-based drug delivery systems - exploring impact of lipid composition type and drug properties on supersaturability and physical stability. *Drug Development and Industrial Pharmacy*, 46, 356-364.
- Jarkko, R., et al. 2008. Prodrugs: Design and clinical applications. *Nature Reviews Drug Discovery*, 7, 255.
- Jerrold, R. T. 2009. Intestinal mucosal barrier function in health and disease. *Nature Reviews Immunology*, 9, 799.
- Kadia, A., et al. 2014. Effects of agitation on particle-size distribution and enzymatic hydrolysis of pretreated spruce and giant reed. *Biotechnology for Biofuels*, 7, 77.
- Kansy, M., et al. 1998. Physicochemical high throughput screening: Parallel artificial membrane permeation assay in the description of passive absorption processes. *Journal of Medicinal Chemistry*, 41, 1007-1010.
- Kazi, M., et al. 2019. Evaluation of self-nanoemulsifying drug delivery systems (SNEDDS) for poorly water-soluble Talinolol: Preparation, in vitro and in vivo Assessment. *Frontiers in Pharmacology*, 10, 459.
- Keemink, J. and Bergström, C. 2018. Caco-2 cell conditions enabling studies of drug absorption from digestible lipid-based formulations. *An Official Journal of the American Association of Pharmaceutical Scientists*, 35, 1-11.
- Keemink, J., et al. 2019. Lipolysis-permeation setup for simultaneous study of digestion and absorption in vitro. *Molecular Pharmaceutics*, 16, 921-930.
- Khadra, I., et al. 2015. Statistical investigation of simulated intestinal fluid composition on the equilibrium solubility of biopharmaceutics classification system class II drugs. *European Journal of Pharmaceutical Sciences*, 67, 65-75.
- Khan, J., et al. 2016. The precipitation behavior of poorly water-soluble drugs with an emphasis on the digestion of lipid based formulations. *An Official Journal of the American Association of Pharmaceutical Scientists*, 33, 548-562.
- Kleberg, K., et al. 2010. Characterising the behaviour of poorly water soluble drugs in the intestine: Application of biorelevant media for solubility, dissolution and transport studies. *Journal of Pharmacy and Pharmacology*, 62, 1656-1668.
- Klitgaard, M., et al. 2019. Improving predictability of oral absorption of lipid-based drug delivery systems through combined intestinal in vitro lipolysis and permeation (LipoPerm). Article in preparation.
- Koziolek, M., et al. 2018. Lipids in the stomach – Implications for the evaluation of food effects on oral drug absorption. *An Official Journal of the American Association of Pharmaceutical Scientists*, 35, 1-26.
- Larsen, A. T., et al. 2011. In vitro lipolysis models as a tool for the characterization of oral lipid and surfactant based drug delivery systems. *International Journal of Pharmaceutics*, 417, 245-255.

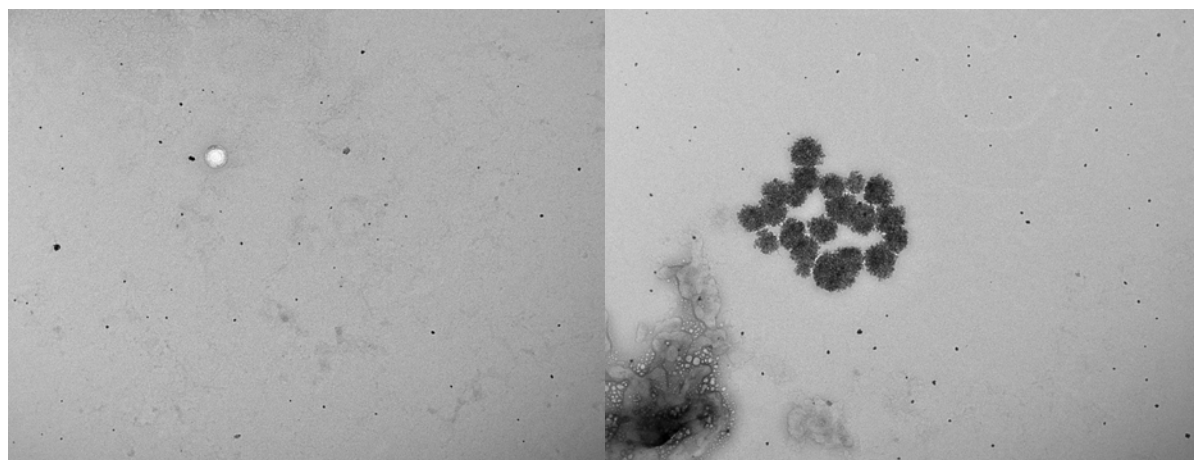
- Lipinski, C. A., et al. 2012. Experimental and computational approaches to estimate solubility and permeability in drug discovery and development settings. *Advanced Drug Delivery Reviews*, 64, 4-17.
- Loftsson, T., et al. 2006. Influence of aqueous diffusion layer on passive drug diffusion from aqueous cyclodextrin solutions through biological membranes. *Die Pharmazie*, 61, 83-89.
- Macierzanka, A., et al. 2019. Bile salts in digestion and transport of lipids. *Advances in Colloid and Interface Science*, 274, 102045.
- McClements, D. J. and Li, Y. 2010. Review of in vitro digestion models for rapid screening of emulsion-based systems. *Food & Function*, 1, 32-59.
- Michaelsen, M. H., et al. 2019. Fenofibrate oral absorption from SNEDDS and super-SNEDDS is not significantly affected by lipase inhibition in rats. *European Journal of Pharmaceutics and Biopharmaceutics*, 142, 258-264.
- Mosgaard, M. D., et al. 2015. Development of a high-throughput in vitro intestinal lipolysis model for rapid screening of lipid-based drug delivery systems. *European Journal of Pharmaceutics and Biopharmaceutics*, 94, 493-500.
- Mosgaard, M. D., et al. 2017. High-throughput lipolysis in 96-well plates for rapid screening of lipid-based drug delivery systems. *Journal of Pharmaceutical Sciences*, 106, 1183-1186.
- Mudie, D. M., et al. 2010. Physiological parameters for oral delivery and in vitro testing. *Molecular Pharmaceutics*, 7, 1388-1405.
- Murgia, X., et al. 2018. The role of mucus on drug transport and its potential to affect therapeutic outcomes. *Advanced Drug Delivery Reviews*, 124, 82-97.
- Müllertz, A., et al. 2010. New perspectives on lipid and surfactant based drug delivery systems for oral delivery of poorly soluble drugs. 62, 1622-1636.
- Noyes, A. A. and Whitney, W. R. 1897. The rate of solution of solid substances in their own solutions. *Journal of the American Chemical Society*, 19, 930-934.
- Patrick, G. L. 2013. *An introduction to medicinal chemistry*. 5th edition. Oxford: Oxford University Press.
- Persson, E., et al. 2005. The effects of food on the dissolution of poorly soluble drugs in human and in model small intestinal fluids. *An Official Journal of the American Association of Pharmaceutical Scientists*, 22, 2141-2151.
- Poovi, G. and Damodharan, N. 2018. Lipid nanoparticles: A challenging approach for oral delivery of BCS Class-II drugs. *Future Journal of Pharmaceutical sciences*, 4, 191-205.
- Porter, C., et al. 2007. Lipids and lipid-based formulations: optimizing the oral delivery of lipophilic drugs. *Nature Reviews Drug Discovery*, 6, 231-248.
- Porter, C. J. H., et al. 2008. Enhancing intestinal drug solubilisation using lipid-based delivery systems. *Advanced Drug Delivery Reviews*, 60, 673-691.
- Pouton, C. W. 2000. Lipid formulations for oral administration of drugs: Non-emulsifying, self-emulsifying and 'self-microemulsifying' drug delivery systems. *European Journal of Pharmaceutical Sciences*, 11, 93-98.
- Pouton, C. W. 2006. Formulation of poorly water-soluble drugs for oral administration: Physicochemical and physiological issues and the lipid formulation classification system. *European Journal of Pharmaceutical Sciences*, 29, 278-287.
- Qiu, Y., et al. 2017. *Developing solid oral dosage forms*. 2nd edition. London: Academic Press.
- Rang, H. P., et al. 2016. *Rang and Dale's pharmacology*. 8th edition. Edinburgh: Churchill Livingstone.
- Rezhdo, O., et al. 2016. Lipid-associated oral delivery: Mechanisms and analysis of oral absorption enhancement. *Journal of Controlled Release*, 240, 544-560.

- Salvia-Trujillo, L., et al. 2013. Influence of particle size on lipid digestion and β -carotene bioaccessibility in emulsions and nanoemulsions. *Food Chemistry*, 141, 1472-1480.
- Sassene, P., et al. 2014. Toward the establishment of standardized in vitro tests for lipid-based formulations, part 6: effects of varying pancreatin and calcium levels. *An Official Journal of the American Association of Pharmaceutical Scientists*, 16, 1344-1357.
- Sastry, S. V., et al. 2000. Recent technological advances in oral drug delivery – a review. *Pharmaceutical Science & Technology Today*, 3, 138-145.
- Sherwood, L. 2013. *Introduction to human physiology*. 8th edition. Independence: Cengage Learning.
- Sigurðsson, H. H., et al. 2013. Mucus as a barrier to lipophilic drugs. *International Journal of Pharmaceutics*, 453, 56-64.
- Siqueira, S., et al. 2017. Influence of drug load and physical form of cinnarizine in new SNEDDS dosing regimens: in vivo and in vitro evaluations. *An Official Journal of the American Association of Pharmaceutical Scientists*, 19, 587-594.
- Thomas, N., et al. 2013. Supersaturated Self-Nanoemulsifying Drug Delivery Systems (Super-SNEDDS) Enhance the Bioavailability of the Poorly Water-Soluble Drug Simvastatin in Dogs. *An Official Journal of the American Association of Pharmaceutical Scientists*, 15, 219-227.
- Thomas, N., et al. 2012a. In vitro and in vivo performance of novel supersaturated self-nanoemulsifying drug delivery systems (super-SNEDDS). *Journal of Controlled Release*, 160, 25-32.
- Thomas, N., et al. 2012b. Influence of lipid composition and drug load on the In Vitro performance of self-nanoemulsifying drug delivery systems. *Journal of Pharmaceutical Sciences*, 101, 1721-1731.
- Thomas, N., et al. 2014. In vitro lipolysis data does not adequately predict the in vivo performance of lipid-based drug delivery systems containing fenofibrate. *The American Association of Pharmaceutical Scientists Journal*, 16, 539-549.
- Thuenemann, E. C., et al. 2015. Dynamic gastric model (DGM). *The Impact of Food Bioactives on Health: In Vitro and Ex Vivo Models*. Springer International Publishing.
- Tran, T., et al. 2017. Monoacyl phosphatidylcholine inhibits the formation of lipid multilamellar structures during in vitro lipolysis of self-emulsifying drug delivery systems. *European Journal of Pharmaceutical Sciences*, 108, 62-70.
- Veber, D. F., et al. 2002. Molecular Properties That Influence the Oral Bioavailability of Drug Candidates. *Journal of Medicinal Chemistry*, 45, 2615-2623.
- Vertzoni, M., et al. 2019. Impact of regional differences along the gastrointestinal tract of healthy adults on oral drug absorption: An UNGAP review. *European Journal of Pharmaceutical Sciences*, 134, 153-175.
- Wilde, P. J. and Chu, B. S. 2011. Interfacial & colloidal aspects of lipid digestion. *Advances in colloid and interface science*, 165, 14-22.
- Williams, H. D., et al. 2013. Toward the establishment of standardized in vitro tests for lipid-based formulations, part 3: understanding supersaturation versus precipitation potential during the in vitro digestion of type I, II, IIIA, IIIB and IV lipid-based formulations. *Pharmaceutical research*, 30, 3059-3076.
- Yeagle, P. L. 2016. *The membranes of cells*. 3rd edition. Amsterdam: Academic Press.
- Zangenberg, N. H., et al. 2001. A dynamic in vitro lipolysis model: I. Controlling the rate of lipolysis by continuous addition of calcium. *European Journal of Pharmaceutical Sciences*, 14, 115-122.

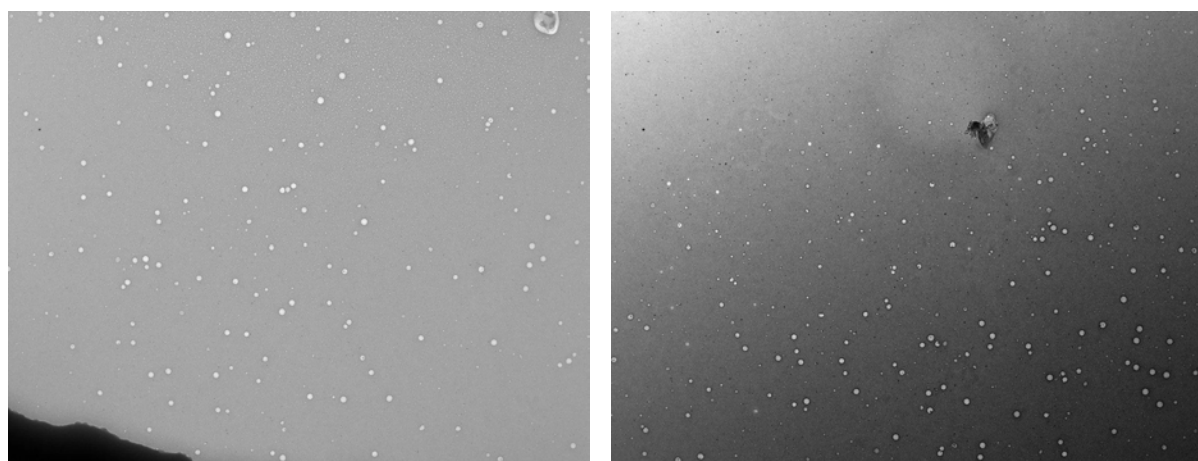
APPENDIX

Transmission electron microscopy

Samples of SNEDDS dispersed in HTP medium with calcein and fasted state intestinal medium with calcein were characterized with a transmission electron microscopy (TEM) (HT7800 Hitachi TEM). TEM images obtained for SNEDDS dispersed in HTP medium with calcein are presented in **Appendix Figure 1** and TEM images obtained for SNEDDS dispersed in fasted state intestinal medium with calcein are presented in **Appendix Figure 2**.



Appendix Figure 1: TEM images of SNEDDS dispersed in HTP medium with calcein.



Appendix Figure 2: TEM images of SNEDDS dispersed in fasted state intestinal medium with calcein.

